Advanced Steel Construction – Vol. 15 No. 4 (2019) 349–363
DOI:10.18057/IJASC.2019.15.4.6

MODIFICATIONS TO THE GLOBAL AND INTERACTIVE SHEAR BUCKLING ANALYSIS METHODS OF TRAPEZOIDAL CORRUGATED STEEL WEBS FOR BRIDGES

Su-mei Liu [1, 2], Han-shan Ding [1, *], Luc Taerwe [2, 3] and Wouter De Corte [2]

[1] *School of Civil Engineering, Southeast University, Nanjing, 211189, China*
[2] *Department of Structural Engineering, Faculty of Engineering and Architecture, Ghent University, Ghent, 9000, Belgium*
[3] *College of Civil Engineering, Tongji University, Shanghai, 200092, China*
* *(Corresponding author: E-mail: hsding@seu.edu.cn)*

A B S T R A C T

The value of the global shear buckling coefficient k_g and the formula for the interactive shear buckling stress of corrugated steel webs (CSWs) are still the subject of debate. In this study, firstly, the analytical formulas for the global and interactive shear buckling stresses of CSWs are deduced by the Galerkin method. Simplified formulas for the global shear buckling coefficient k_g for a four-edge simple support, for a four-edge fixed support, for two edges constrained by flanges fixed and the other two edges simply supported, and an interactive shear buckling coefficient table are given. Secondly, an elastic finite element analysis is carried out to verify the analytical formulas and to study the influence of geometric parameters on the shear buckling stress of CSWs. Finally, a design formula for the shear strength of CSWs which adopts the formulas for the global and interactive shear buckling stresses proposed in this paper is assessed. From a comparison between the shear strength calculated by this design formula, calculated by four previous design formulas and measured in a series of published test results, it is found that the considered design formula provides good predictions for the shear strength of CSWs and can be recommended.

A R T I C L E H I S T O R Y

Received: 15 January 2019
Revised: 07 June 2019
Accepted: 13 June 2019

K E Y W O R D S

Corrugated steel web;
Global shear buckling;
Interactive shear buckling;
Shear strength;
Galerkin method;
Finite element analysis

1. Introduction

The steel-concrete composite girder with corrugated steel webs (CSWs) (see Fig. 1) is known as a new type of bridge structure to overcome the weight problem of common concrete box girders. Compared with concrete webs, CSWs have low longitudinal stiffness due to the accordion effect, so CSWs mainly carry the shear forces and barely carry axial forces [1]. Because of this characteristic, CSWs fail due to shear buckling or yielding [2]. Therefore, the shear buckling stability of CSWs is one of the most important considerations in the design of this kind of composite girder bridges.

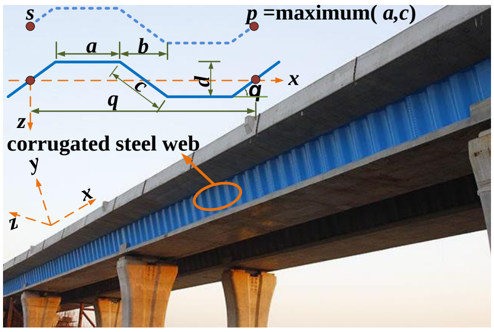

Fig. 1 Composite girder with CSWs

It is widely accepted that local buckling is the primary failure mode in coarse corrugations, whereas global buckling becomes the primary failure mode in dense corrugations and interactive shear buckling mode becomes primary when the density is in between of the two above scenarios [3].

The local shear buckling of CSWs is solved by analyzing a single flat panel constrained by adjacent panels and girder flanges. For this, the shear buckling stress formula of isotropic rectangular plates [4] can be applied. Aggarwal et al. [5] numerically investigated the local shear buckling of CSWs and found that the edge conditions between the CSWs and the girder flanges were close to fixed, while those between the flat and inclined panels lied between simply supported and fixed.

The global shear buckling of CSWs for straight girder bridges is analyzed by treating the whole corrugated steel web (CSW) as an orthotropic rectangular plate constrained by concrete flanges and diaphragms, and has been studied by various researchers. Easley and McFarland [6] investigated the global shear buckling behavior of corrugated metal diaphragms by assuming them as orthotropic plates and developed the formula for the shear buckling load by the Ritz and the Energy method. Then, Easley [7] made a comparative analysis of the Bergmann-Reissner formula [8], the Hlavacek formula [9] and the Easley-McFarland formula [6], and proposed a more comprehensive and applicable global shear buckling formula of corrugated plates. As application of corrugated plates, initially used for aircrafts, was gradually extended to civil engineering, the formula $\tau_g^e = k_g \dfrac{(D_x)^{1/4}(D_y)^{3/4}}{th^2}$ was accepted to calculate the global shear buckling stress of CSWs, where k_g is the global shear buckling coefficient depending on the edge conditions. For a four-edge simple support, Easley [7] suggested k_g=36, Peterson [10] and Bergfelt et al. [11] suggested k_g=32.4, while the Guide to Stability Design Criteria for Metal Structures [12] adopts k_g=31.6. For a four-edge fixed support, Easley [7] suggested k_g=68.4, Peterson [10] and Bergfelt, et al. [11] suggested k_g=60.4, while the Guide to Stability Design Criteria for Metal Structures [12] adopts k_g=59.2. El Metwally and Loov [13] suggested k_g=50 for composite girders with CSWs. From the studies mentioned above, it is clear that although a global shear buckling formula of CSWs has been proposed, researchers hold different views on the value of the global shear buckling coefficient k_g. Many adjustments of the coefficient k_g are based on FEA only, and lack theoretical support. Machimdamrong et al. [14] presented the transition curves of the elastic global shear buckling capacity with the boundary conditions from a four-edge simple support to a four-edge fixed support using the Rayleigh-Ritz method, but only the curves for the plate dimensions (l×h) of 1m×1m and 2m×1m were provided. Therefore, it is necessary to investigate the global shear buckling of CSWs with different boundary conditions theoretically.

Finally, the formula for the interactive shear buckling is determined by the local and global shear buckling stresses, and the yield stress of the plate material [15], but the way these parameters are to be combined is still the subject of debate. Important work has been done by Bergfelt and Leiva-Aravena [16], El Metwally [17], Abbas et al. [18], Shiratani et al. [19], Sayed-Ahmed [20] and Yi et al. [15], etc., and various interactive shear buckling formulas of CSWs were proposed. All the formulas might be not accurate enough since their forms were too simple [21], and are based on the relationship between the local and global shear buckling stresses, and the yield stress only. All the elastic interactive formulas show that the interactive shear buckling stress is the minimum value of the three shear buckling modes, which is not reasonable and lacks theoretical support. Therefore, it is necessary to investigate the interactive shear buckling of CSWs from a theoretical point of view.

For practical applications, Elgaaly et al. [22] recommended that the capacity of CSWs was controlled by the minimum value of local and global buckling stresses, and a semiempirical formula for the inelastic buckling stress was proposed. Driver et al. [23] suggested a lower bound formula by combining local and global shear buckling formulas. Moon et al. [24] proposed a shear buckling parameter formula for trapezoidal CSWs based on the relationship between local, global and interactive shear buckling stresses. Eldib [3] proposed a shear buckling parameter formula for curved CSWs. Nie et al. [21] carried out eight H-shape steel girders with CSWs and suggested a formula for the shear strength prediction of trapezoidal CSWs. Hassanein et al. studied the shear behavior of linearly tapered girder bridges with CSWs [25], and girders with high-strength CSWs [26]. Leblouba and Barakat [2] experimentally and numerically investigated the shear stress distribution in trapezoidal CSWs.

In this study, the whole CSW is treated as an orthotropic plate constrained by flanges and diaphragms for the global shear buckling analysis, and the folded plate composed of two adjacent panels is treated as an isotropic shallow shell for the interactive shear buckling analysis. Firstly, the analytical formulas for the global and interactive shear buckling stresses are derived by the Galerkin method. Then, an elastic finite element analysis (FEA) is carried out to verify the analytical formulas and to study the influence of geometric parameters on the shear buckling stress of CSWs. Finally, a design formula for the shear strength of CSWs which adopts the formulas for the global and interactive shear buckling stresses proposed in this paper is assessed.

2. Elastic shear buckling stress of CSWs

2.1. Physical equivalent parameters of CSWs

For trapezoidal CSWs that are commonly used in actual girder bridges, when treated as an orthotropic plate, the equivalent flexural stiffnesses D_x, D_y and the torsional stiffness D_{xy} per unit length of a CSW can be expressed as Eqs. (1)-(3) [6].

$$D_x = \frac{q}{s}\frac{Et^3}{12} = \frac{Et^3\left(2a+2d.\cot\theta\right)}{12\left(2a+2d.\csc\theta\right)} \tag{1}$$

$$D_y = \frac{Etd^2\left(3a+c\right)}{6q} = \frac{Etd^2\left(3a+d.\csc\theta\right)}{6\left(2a+2d.\cot\theta\right)} \tag{2}$$

$$D_{xy} = \frac{s}{q}\frac{Et^3}{6(1+\mu)} = \frac{Et^3\left(2a+2d.\csc\theta\right)}{6(1+\mu)\left(2a+2d.\cot\theta\right)} \tag{3}$$

where E is the elastic modulus of the original steel plate; μ is the Poisson's ratio; t is the web thickness. As shown in Fig. 1, a is the flat panel width; c is the inclined panel width; d is the corrugation depth; θ is the corrugation angle; q is the horizontal projection length of one periodic corrugation; s is the total folded panel length of one periodic corrugation.

2.2. Elastic local shear buckling

The shear buckling stress formula of isotropic rectangular plates Eq. (4) [4] can be applied to calculate the elastic local shear buckling stress of CSWs.

$$\tau_l^e = k_l \frac{\pi^2 E}{12\left(1-\mu^2\right)}\left(\frac{t}{p}\right)^2 \tag{4}$$

where k_l is the elastic local shear buckling coefficient of CSWs; p is the maximum value of the flat panel width a and the inclined panel width c.

The elastic local shear buckling coefficient k_l can be expressed as Eqs. (5)-(7).

For a four-edge simple support:

$$k_{l,s} = 5.34 + 4\left(p/h\right)^2 \tag{5}$$

For a four-edge fixed support:

$$k = 8.98 + 5.6\left(p/h\right) \tag{6}$$

For the two edges constrained by flanges fixed and the other two edges simply supported:

$$k_{l,fs} = 5.34 + 2.31\left(p/h\right) - 3.44\left(p/h\right)^2 + 8.39\left(p/h\right)^3 \tag{7}$$

2.3. Elastic global shear buckling

2.3.1. Critical buckling stress under pure shear

A CSW with dense corrugations can be treated as an orthotropic plate (Fig. 2) for the global shear buckling analysis.

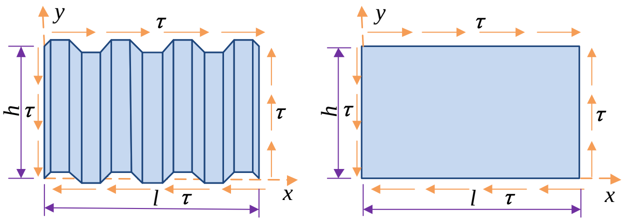

(a) CSW (b) Equivalent orthotropic plate

Fig. 2 CSW and its equivalent orthotropic plate

According to the stability theory of plates, the equilibrium equation of an orthotropic plate subjected to a shear force can be expressed as Eq. (8) [27].

$$\frac{1}{t}\left(D_x\frac{\partial^4}{\partial x^4} + D_{xy}\frac{\partial^4}{\partial x^2\partial y^2} + D_y\frac{\partial^4}{\partial y^4}\right)w = 2\tau\frac{\partial^2 w}{\partial x\partial y} \tag{8}$$

where w is the out of plane deflection of the plate, τ is the shear stress.

It can be assumed that the boundary conditions of CSWs satisfy a four-edge simple support, a four-edge fixed support, or two edges constrained by flanges fixed and the other two edges simply supported (the edges x=0 and x=l are simply supported, the edges y=0 and y=h are fixed supported). The functions of deflection can be expressed respectively as Eqs. (9)-(11).

For a four-edge simple support [4]:

$$w = \sum_{m=1}^{\infty}\sum_{n=1}^{\infty} C_{mn}\sin\frac{m\pi x}{l}\sin\frac{n\pi y}{h} \tag{9}$$

For a four-edge fixed support [28]:

$$w = \sum_{m=1}^{\infty}\sum_{n=1}^{\infty} C_{mn}\left(\frac{1}{m}\sin\frac{m\pi x}{l} - \frac{1}{m+2}\sin\frac{(m+2)\pi x}{l}\right)\left(\frac{1}{n}\sin\frac{n\pi y}{h} - \frac{1}{n+2}\sin\frac{(n+2)\pi y}{h}\right) \tag{10}$$

For the edges x=0 and x=l simply supported, and the edges y=0 and y=h fixed:

$$w = \sum_{m=1}^{\infty}\sum_{n=1}^{\infty} C_{mn}\sin\frac{m\pi x}{l}\left(\frac{1}{n}\sin\frac{n\pi y}{h} - \frac{1}{n+2}\sin\frac{(n+2)\pi y}{h}\right) \tag{11}$$

where h is the web height equal to the clear distance between the top and bottom concrete flanges, l is the web length equal to the distance between the two adjacent diaphragm plates.

Given λ=l/h, α=D_x/D_y and β=D_{xy}/D_y, Eq. (8) can be simplified as Eqs. (12)-(14) according to the Galerkin method.

For the four-edge simple support:

$$\frac{\pi^4 D_y}{4th^2\lambda^3}\left(\alpha m^4 + \beta m^2 n^2\lambda^2 + n^4\lambda^4\right)C_{mn} - 8\tau\sum_{i=1}^{\infty}\sum_{j=1}^{\infty} C_{ij}\frac{mnij}{\left(m^2-i^2\right)\left(n^2-j^2\right)} = 0$$
$$\left(m \pm i = \text{odd number},\ n \pm j = \text{odd number}\right) \tag{12}$$

For the four-edge fixed support:

$$
\frac{D_y}{th^2}\frac{\pi^4}{4\lambda^3}\left\{\begin{array}{l}
C_{mn}\left\{\begin{array}{l}\alpha\left[m^2+(m+2)^2\right]\left[n^{-2}+(n+2)^{-2}\right]+4\beta\lambda^2\\ +\lambda^4\left[m^{-2}+(m+2)^{-2}\right]\left[n^2+(n+2)^2\right]\end{array}\right\}\\
-C_{m,n+2}\left\{\alpha\left[m^2+(m+2)^2\right](n+2)^{-2}+2\beta\lambda^2+\lambda^4\left[m^{-2}+(m+2)^{-2}\right](n+2)^2\right\}\\
-C_{m,n-2}\left\{\alpha\left[m^2+(m+2)^2\right]n^{-2}+2\beta\lambda^2+\lambda^4\left[m^{-2}+(m+2)^{-2}\right]n^2\right\}\\
-C_{m+2,n}\left\{\alpha(m+2)^2\left[n^{-2}+(n+2)^{-2}\right]+2\beta\lambda^2+\lambda^4(m+2)^{-2}\left[n^2+(n+2)^2\right]\right\}\\
+C_{m+2,n+2}\left[\alpha(m+2)^2(n+2)^{-2}+\beta\lambda^2+\lambda^4(m+2)^{-2}(n+2)^2\right]\\
+C_{m+2,n-2}\left[\alpha(m+2)^2n^{-2}+\beta\lambda^2+\lambda^4(m+2)^{-2}n^2\right]\\
-C_{m-2,n}\left\{\alpha m^2\left[n^{-2}+(n+2)^{-2}\right]+2\beta\lambda^2+\lambda^4m^{-2}\left[n^2+(n+2)^2\right]\right\}\\
+C_{m-2,n+2}\left[\alpha m^2(n+2)^{-2}+\beta\lambda^2+\lambda^4m^{-2}(n+2)^2\right]\\
+C_{m-2,n-2}\left[\alpha m^2n^{-2}+\beta\lambda^2+\lambda^4m^{-2}n^2\right]
\end{array}\right\}
$$

$$
-8\tau\sum_{i=1}^{\infty}\sum_{j=1}^{\infty}A_{ij}\left\{\begin{array}{l}\left[\frac{1}{m^2-i^2}-\frac{1}{(m+2)^2-i^2}-\frac{1}{m^2-(i+2)^2}+\frac{1}{(m+2)^2-(i+2)^2}\right]\\ \times\left[\frac{1}{n^2-j^2}-\frac{1}{(n+2)^2-j^2}-\frac{1}{n^2-(j+2)^2}+\frac{1}{(n+2)^2-(j+2)^2}\right]\end{array}\right\}=0 \quad (13)
$$

$$(m\pm i=\text{odd number},\ n\pm j=\text{odd number})$$

For the edges x=0 and x=l simply supported, and the edges y=0 and y=h fixed:

$$
\frac{D_y}{th^2}\frac{\pi^4}{4\lambda^3}\left\{\begin{array}{l}
C_{mn}\left\{\alpha m^4\left[n^{-2}+(n+2)^{-2}\right]+2\beta\lambda^2m^2+\lambda^4\left[n^2+(n+2)^2\right]\right\}\\
-C_{m,n+2}\left[\alpha m^4(n+2)^{-2}+\beta\lambda^2m^2+\lambda^4(n+2)^2\right]\\
-C_{m,n-2}\left[\alpha m^4n^{-2}+\beta\lambda^2m^2+\lambda^4n^2\right]
\end{array}\right\}
$$

$$
-8\tau\sum_{i=1}^{\infty}\sum_{j=1}^{\infty}A_{ij}\frac{mi}{m^2-i^2}\left[\begin{array}{l}\frac{1}{n^2-j^2}-\frac{1}{(n+2)^2-j^2}-\frac{1}{n^2-(j+2)^2}\\ +\frac{1}{(n+2)^2-(j+2)^2}\end{array}\right]=0 \quad (14)
$$

$$(m\pm i=\text{odd number},\ n\pm j=\text{odd number})$$

By assigning values to m and n in Eqs. (12)-(14), a series of linear algebraic equations with C_{ij} as unknowns can be obtained. Then the critical shear buckling stress can be derived by assuming the coefficient determinant of the linear algebraic equations equals zero. (i. e. a linear bifurcation analysis).

According to Eqs. (12)-(14), the elastic global shear buckling stress of CSWs can be expressed as Eq. (15).

$$\tau_g^e=k_g\frac{D_y}{h^2t} \quad (15)$$

where k_g is the elastic global shear buckling coefficient of CSWs. The detailed solution process of the coefficient $k_{g,s}$ for a four-edge simple support, $k_{g,f}$ for a four-edge fixed support, $k_{g,fs}$ for the edges x=0 and x=l simply supported, and the edges y=0 and y=h fixed is given below.

2.3.2. Calculation of the global shear buckling coefficient k_g

(1) Comparison with isotropic plate

Based on "Theory of elastic stability" [4], the elastic shear buckling stress of isotropic rectangular plates can be expressed as Eq. (16).

$$\tau_{cr}^e=k\frac{\pi^2D}{h^2t} \quad (16)$$

where D is the flexural stiffness, and k is the elastic shear buckling coefficient of isotropic rectangular plates. The coefficients k_s for the four-edge simple support, k_f for the four-edge fixed support, k_{fs} for the edges x=0 and x=l simply supported, and the edges y=0 and y=h fixed are given in Timoshenko [4].

When D_x/D_y=1 and D_{xy}/D_y=2, The Eq. (15) for the elastic global shear buckling stress of CSWs derived in this paper can be also applied to calculate isotropic plates. The global shear buckling coefficient k_g in Eq. (15) should be divided by π^2 to meet the needs of comparison with Timoshenko [4]. The shear buckling coefficient k from Timoshenko [4] and k_g/π^2 derived in this paper are given in Table 1.

As can be seen from Table 1, the average difference between k_g/π^2 derived in this paper, which takes 900 trigonometric series (m=30, n=30), and k from Timoshenko [4] is 1.2% (the maximum being 4.4%) showing the accuracy of the solution method proposed in this paper.

Table 1

Elastic shear buckling coefficient of isotropic rectangular plates

Coefficient	Boundaries	l/h									
		1	1.2	1.4	1.5	1.6	1.8	2	2.5	3	4
$k_{g,s}/\pi^2$	Four-edge simply	9.32	7.98	7.29	7.07	6.91	6.69	6.55	6.08	5.84	5.62
k_s		9.34	8	7.3	7.1	7	6.8	6.6	6.1	5.9	5.7
$k_{g,f}/\pi^2$	Four-edge fixed	15.04	—	—	11.77	—	—	10.52	—	—	—
k_f		14.71	—	—	11.5	—	—	10.34	—	—	—
$k_{g,fs}/\pi^2$	x=0, x=l simply,	12.82	—	—	11.01	—	—	10.26	9.88	9.73	—
k_{fs}	y=0, y=h fixed	12.28	—	—	11.12	—	—	10.21	9.81	9.61	—

Note: "—" expresses the value of k is not given in Timoshenko [4].

Table 2

Geometry of CSWs in actual bridges [3, 15, 24, 26, 29]

Bridges	a	b	c	d	h	t_{min}	t_{max}	$\frac{a}{t_{min}}$	$\frac{a}{t_{max}}$	$\frac{3a+c}{q}$	Based on t_{min}		Based on t_{max}	
	mm	mm	mm	mm	mm	mm	mm				α	β	α	β
Cognac	353	319	353	150	1771	8	8	44.1	44.1	1.05	0.0013	0.0022	0.0013	0.0022
Maupre	284	241	284	150	2650	8	8	35.5	35.5	1.08	0.0012	0.0022	0.0012	0.0022
Dole	430	370	430	220	1800~4010	8	12	53.8	35.8	1.08	0.0006	0.0010	0.0013	0.0023
Shinkai	250	200	250	150	1183	9	9	27.8	27.8	1.11	0.0015	0.0028	0.0015	0.0028
Miyukibashi	300	260	300	150	2210	8	12	37.5	25.0	1.07	0.0012	0.0022	0.0028	0.0049
Katsutegawa	430	370	430	220	2080~5300	9	12	47.8	35.8	1.08	0.0007	0.0013	0.0013	0.0023
Hondani	330	270	336	200	1025~5095	9	14	36.7	23.6	1.11	0.0008	0.0016	0.0020	0.0038
Koinumarukawa	430	370	430	220	1580~3600	9	16	47.8	26.9	1.08	0.0007	0.0013	0.0023	0.0041
Shimoda	430	370	430	220	1140~5360	12	16	35.8	26.9	1.08	0.0013	0.0023	0.0023	0.0041
Nakano Viaduct	330	270	336	200	1010~3100	9	19	36.7	17.4	1.11	0.0008	0.0016	0.0037	0.0070
Kurobekawa Railway	400	350	400	200	2500~3400	12	25	33.3	16.0	1.07	0.0016	0.0028	0.0069	0.0120
Altwipfergrund	360	288	360	220	1633~2674	10	22	36.0	16.4	1.11	0.0008	0.0016	0.0041	0.0077
Juancheng-Huanghe	430	370	430	220	1729~4253	10	18	43.0	23.9	1.08	0.0009	0.0016	0.0029	0.0051
Henan-Pohe	250	200	250	150	1305	8	8	31.3	31.3	1.11	0.0012	0.0022	0.0012	0.0022
Wei River	330	270	336	200	1000~1350	8	12	41.3	27.5	1.11	0.0007	0.0012	0.0015	0.0028
Nanjing-Chuhe	430	370	430	220	2420~4900	10	18	43.0	23.9	1.08	0.0009	0.0016	0.0029	0.0051

Note: t_{max} and t_{min} are the maximum and minimum thicknesses of CSWs respectively when an actual bridge has more than one thickness value.

(2) Calculation of k_g

According to Eqs. (12)-(15), the global shear buckling coefficient k_g is associated with the length to height ratio λ (l/h), and the rigidity ratios α (D_x/D_y) and β (D_{xy}/D_y). A statistical analysis of available bridges with CSWs (as shown in Table 2) shows that the rigidity ratio α varies from 0.0006 to 0.0069, whereas β is about (1.67~2.0)α. The following parametric study considers α ranging from 0.0005 to 0.0070, and β equal to 1.6α, 1.8α, 2.0α respectively.

Theoretically, the more numbers used in the trigonometric series (as shown in Eqs. (9)-(11)), the more precise the solution is. If m and n increase toward infinity, exact results of shear buckling stress can be obtained. However, the calculation effort increases with the increasing numbers m and n in the trigonometric series. In the case of the CSW with a length to height ratio l/h less than 5, the deviation between the results with m=30, n=30 and the results with m=25, n=25 is less than 1%. So, adopting m=30 and n=30 for further calculation will not only ensure the accuracy of the calculation but also reduce the calculation effort.

Table 3 shows the values of $k_{g,s}$ calculated for various values of D_x/D_y and l/h, and for β=1.6α, β=1.8α and β=2.0α respectively for a four-edge simple support. The results for β=1.6α and β=2.0α, compared to for β=1.8α, deviate less than 0.6%. The results show that the parameter β/α has little effect on the coefficient k_g for common bridges with CSWs. From an engineering application point of view, the deviations can be ignored. In addition, the conclusion remains unchanged for a four-edge fixed support, and for two edges constrained by flanges fixed and the other two edges simply supported. As a result, β=1.8α is used further in this paper.

Tables 4-6 list the values of the global shear buckling coefficient k_g for length to height ratios l/h varying from 1 to 5, a rigidity ratio D_x/D_y varying from 0.0005 to 0.0070, and a fixed value of β=1.8α. As shown in Tables 4 to 6, global shear buckling coefficients $k_{g,s}$, $k_{g,f}$, and $k_{g,fs}$ for an equal web length to height ratio l/h and rigidity ratio D_x/D_y exhibit relationships: $k_{g,f}/k_{g,s}$=1.84~1.90, $k_{g,fs}/k_{g,s}$=1.83~1.89, $k_{g,f}/k_{g,fs}$=1~1.013. This shows that the global shear buckling stress for the four-edge fixed support is only slightly higher than for two edges constrained by flanges fixed and the other two edges simply supported, the difference is less than 1.5%.

Table 3

The effect of β/α on the global shear buckling coefficient $k_{g,s}$ for the four-edge simple support

D_x/D_y		l/h				
		1	2	3	4	5
0.0005	β=1.6α	5.016	4.947	4.933	4.929	4.927
	β=1.8α	5.024	4.954	4.940	4.936	4.934
	β=2.0α	5.031	4.962	4.948	4.944	4.942
0.0015	β=1.6α	6.729	6.593	6.562	6.550	6.545
	β=1.8α	6.747	6.610	6.579	6.567	6.562
	β=2.0α	6.765	6.627	6.597	6.585	6.579
0.0025	β=1.6α	7.741	7.561	7.509	7.492	7.485
	β=1.8α	7.767	7.586	7.534	7.517	7.510
	β=2.0α	7.793	7.611	7.559	7.542	7.535
0.0035	β=1.6α	8.508	8.269	8.215	8.195	8.185
	β=1.8α	8.543	8.302	8.248	8.227	8.217
	β=2.0α	8.577	8.335	8.280	8.259	8.249
0.0050	β=1.6α	9.526	9.113	9.047	9.020	9.006
	β=1.8α	9.568	9.155	9.090	9.062	9.048
	β=2.0α	9.610	9.198	9.132	9.104	9.090
0.0070	β=1.6α	10.392	10.031	9.919	9.885	9.870
	β=1.8α	10.449	10.085	9.973	9.939	9.924
	β=2.0α	10.507	10.139	10.028	9.993	9.977

Table 4

Global shear buckling coefficient $k_{g,s}$ for a four-edge simple support

l/h	D_x/D_y											
	0.0005	0.001	0.0015	0.002	0.0025	0.003	0.0035	0.004	0.0045	0.005	0.006	0.007
1	5.024	6.047	6.747	7.335	7.767	8.165	8.543	8.903	9.249	9.568	10.025	10.449
1.5	4.975	5.964	6.647	7.186	7.639	8.017	8.371	8.705	9.002	9.255	9.728	10.172
2	4.954	5.937	6.610	7.134	7.586	7.958	8.302	8.624	8.899	9.155	9.638	10.085
2.5	4.945	5.924	6.589	7.113	7.552	7.929	8.268	8.579	8.853	9.112	9.596	10.005
3	4.940	5.914	6.579	7.100	7.534	7.911	8.248	8.553	8.829	9.090	9.556	9.973
4	4.936	5.906	6.567	7.085	7.517	7.893	8.227	8.528	8.806	9.062	9.527	9.939
5	4.932	5.903	6.562	7.079	7.510	7.884	8.217	8.517	8.794	9.048	9.510	9.924

Table 5

Global shear buckling coefficient $k_{g,f}$ for a four-edge fixed support

l/h	D_x/D_y											
	0.0005	0.001	0.0015	0.002	0.0025	0.003	0.0035	0.004	0.0045	0.005	0.006	0.007
1	9.454	11.352	12.654	13.666	14.533	15.297	15.946	16.546	17.109	17.642	18.616	19.428
1.5	9.392	11.242	12.502	13.494	14.314	15.039	15.669	16.247	16.785	17.273	18.153	18.954
2	9.370	11.204	12.451	13.427	14.240	14.950	15.573	16.143	16.662	17.140	18.016	18.784
2.5	9.360	11.187	12.428	13.397	14.207	14.909	15.529	16.093	16.606	17.083	17.942	18.712
3	9.357	11.178	12.415	13.382	14.188	14.887	15.505	16.065	16.577	17.051	17.908	18.668
4	9.354	11.170	12.409	13.368	14.171	14.865	15.482	16.039	16.548	17.020	17.871	18.628
5	9.352	11.165	12.402	13.359	14.163	14.856	15.473	16.029	16.538	17.007	17.856	18.610

Table 6
Global shear buckling coefficient $k_{g,fs}$ for two edges constrained by flanges fixed and the other two edges simply supported

l/h	D_x/D_y											
	0.0005	0.001	0.0015	0.002	0.0025	0.003	0.0035	0.004	0.0045	0.005	0.006	0.007
1	9.442	11.308	12.590	13.614	14.447	15.170	15.841	16.469	16.989	17.470	18.371	19.214
1.5	9.386	11.227	12.483	13.464	14.296	14.996	15.636	16.212	16.725	17.210	18.113	18.878
2	9.366	11.198	12.445	13.419	14.229	14.930	15.558	16.121	16.636	17.121	17.979	18.753
2.5	9.359	11.183	12.423	13.391	14.199	14.898	15.521	16.080	16.595	17.070	17.928	18.691
3	9.356	11.176	12.413	13.378	14.183	14.881	15.500	16.057	16.571	17.041	17.897	18.658
4	9.353	11.168	12.408	13.368	14.170	14.863	15.479	16.036	16.545	17.016	17.866	18.623
5	9.351	11.164	12.401	13.358	14.162	14.855	15.472	16.028	16.537	17.006	17.854	18.607

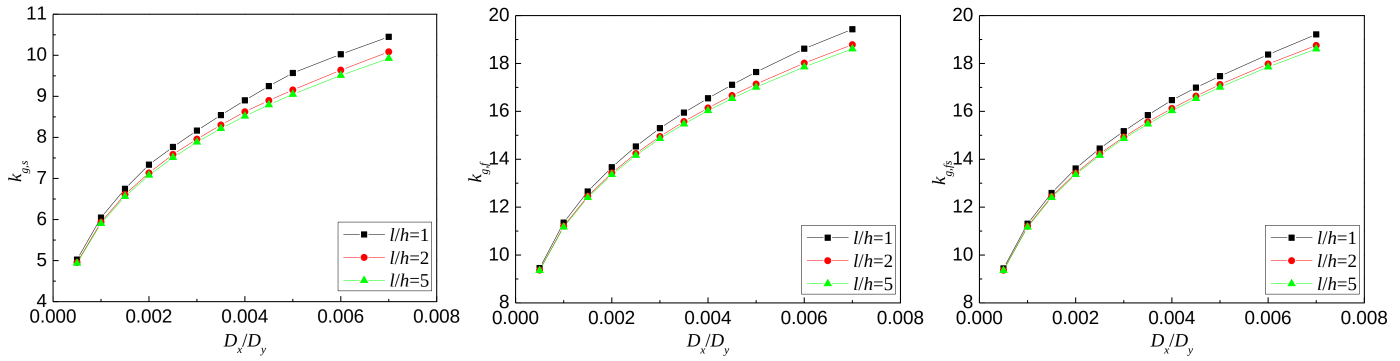

（a）Four-edge simply support (b) Four-edge fixed support (c) Two edges constrained by flanges fixed and the other two edges simply supported

Fig. 3 The effect of the rigidity ratio D_x/D_y on the global shear buckling coefficient k_g

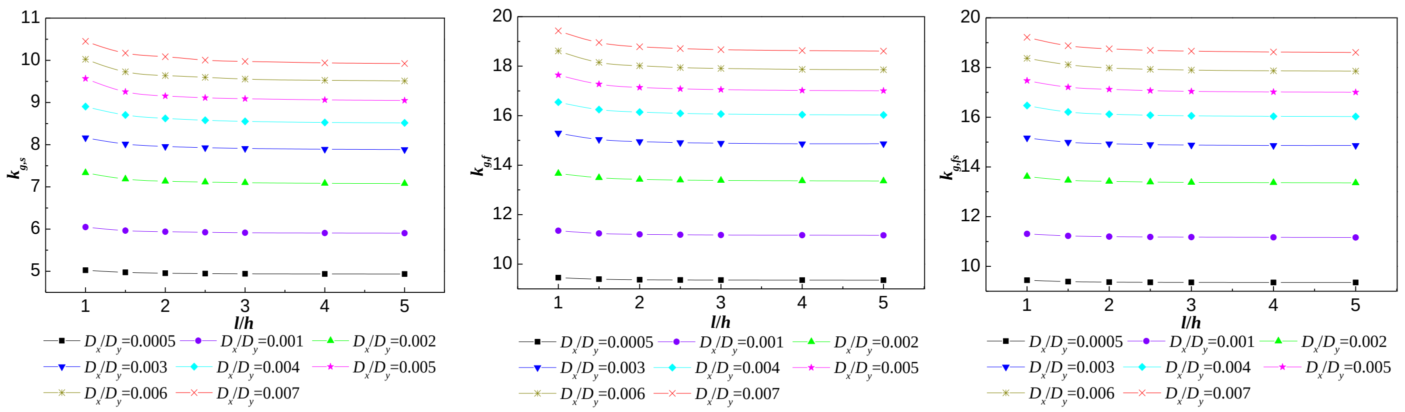

（a）Four-edge simply support (b) Four-edge fixed support (c) Two edges constrained by flanges fixed and the other two edges simply supported

Fig. 4 The effect of the length to height ratio l/h on the global shear buckling coefficient k_g

Table 7
Values of the global shear buckling coefficient k_g for l/h=5

k_g	D_x/D_y													
	0.0005	0.001	0.0015	0.002	0.0025	0.003	0.0035	0.004	0.0045	0.005	0.0055	0.006	0.0065	0.007
$k_{g,s}$	4.932	5.903	6.562	7.079	7.510	7.884	8.217	8.517	8.794	9.048	9.288	9.510	9.722	9.924
$k_{g,f}$	9.352	11.165	12.402	13.359	14.163	14.856	15.473	16.029	16.538	17.007	17.444	17.856	18.242	18.610
$k_{g,fs}$	9.351	11.164	12.401	13.358	14.162	14.855	15.472	16.028	16.537	17.006	17.443	17.854	18.240	18.607

(3) The effect of the rigidity ratio D_x/D_y and the length to height ratio l/h on the global shear buckling coefficient k_g

According to the values of k_g given in Tables 4 to 6, for common bridges with CSWs, Figs. 3-4 show the effect of the web rigidity ratio D_x/D_y and the length to height ratio l/h on the global shear buckling coefficient k_g. As we can see from Figs. 3-4, the global shear buckling coefficient k_g increases with the increase of the rigidity ratio D_x/D_y, and decreases with the increase of the length to height ratio l/h but only very little. When l/h is larger than 2, which is common for CSW bridges, the change of k_g is minimal and the values of k_g show a converging trend.

2.3.3. Elastic global shear buckling stress of CSWs

Substituting Eq. (2) into Eq. (15), the elastic global shear buckling stress of CSWs can be expressed as Eq. (17).

$$\tau_g^e = k_g \frac{E(3a+c)d^2}{6qh^2} = k_g \frac{Ed^2(3a+d.\csc\theta)}{6h^2(2a+2d.\cot\theta)} \tag{17}$$

Because the values of k_g show a converging trend when l/h is larger than 2, we assume l/h=5 for further calculation. This will not only ensure the accuracy of the calculation but also meet the engineering requirements of design simplicity. Table 7 lists the values of k_g for l/h=5.

Through fitting of the data in Table 7, for CSWs with $0.0005 \leqslant \alpha \leqslant 0.0070$, the global shear buckling coefficients $k_{g,s}$, $k_{g,f}$, and $k_{g,fs}$ can be estimated respectively as Eqs. (18) and (19).

For a four-edge simple support:

$$k_{g,s} = 36.8\alpha^{0.2648} \tag{18}$$

For a four-edge fixed support, or for two edges constrained by flanges fixed and the other two edges simply supported:

$$k_{g,f} = k_{g,fs} = 67.7\alpha^{0.2608} \tag{19}$$

For trapezoidal CSWs that are commonly used in actual bridges, the rigidity ratio α can be expressed as Eq. (20).

$$\alpha = \frac{D_x}{D_y} = \frac{q^2 t^2}{2s(3a+c)d^2} = \left(\frac{t}{d}\right)^2 \frac{\left(2a+2d.\cot\theta\right)^2}{2\left(2a+2d.\csc\theta\right)\left(3a+d.\csc\theta\right)} \tag{20}$$

2.4. Elastic interactive shear buckling

2.4.1. Critical buckling stress under pure shear

For the interactive shear buckling analysis, folded plate theory is used. A folded plate structure is a spatial thin wall system with several long and thin plates intersecting. Since interactive shear buckling represents the buckling of a few panels, several panels of CSWs can be treated as a folded plate. For simplicity, the folded plate composed of two adjacent panels shown in Fig. 5 is studied here. According to the theory of thin plates and shells, if $l_3/l_* \leq 0.2$, the folded plate can be analyzed as a shallow shell. CSWs general meet this condition.

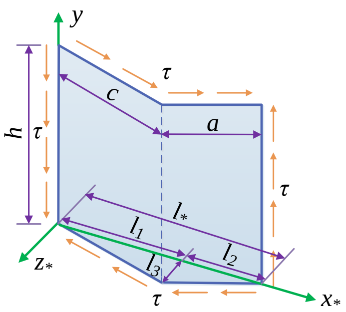

Fig. 5 Shear transfer of interactive shear buckling

In the coordinate system as shown in Fig. 5, the equation for the surface of the shell can be expressed as Eq. (21).

$$z = \frac{l_3}{l_1} x\left[1 - u\left(x - l_1\right)\right] + \frac{l_3}{l_2}\left[\left(l_1 + l_2\right) - x\right] u\left(x - l_1\right) \tag{21}$$

where $u\left(x - l_1\right)$ is the step function and can be expressed as $u(x-l_1) = \begin{cases} 0 & x < l_1 \\ 1 & x \geq l_1 \end{cases}$.

The equilibrium equation and the deformation compatibility equation of a shallow shell under pure shear force can be expressed respectively as Eqs. (22) and (23) [30].

$$\frac{D}{t}\nabla^4 f + \left(k_x \frac{\partial^2}{\partial y^2} - 2k_{xy}\frac{\partial^2}{\partial x \partial y} + k_y \frac{\partial^2}{\partial x^2}\right)\Phi = 2\tau \frac{\partial^2 f}{\partial x \partial y} \tag{22}$$

$$\frac{1}{E}\nabla^4 \Phi - \left(k_x \frac{\partial^2}{\partial y^2} - 2k_{xy}\frac{\partial^2}{\partial x \partial y} + k_y \frac{\partial^2}{\partial x^2}\right) f = 0 \tag{23}$$

where f is the out of plane deflection of the shell, Φ is the stress function, $k_x = -\dfrac{\partial^2 z}{\partial x^2}$, $k_y = -\dfrac{\partial^2 z}{\partial y^2}$, $k_{xy} = -\dfrac{\partial^2 z}{\partial x \partial y}$.

It can be conservatively assumed that the boundary conditions of CSWs for the interactive shear buckling analysis satisfy four-edge simple support. The deflection function and stress function can be expressed respectively as Eqs. (24) and (25).

$$f = \sum_{m=1}^{\infty}\sum_{n=1}^{\infty} A_{mn} \sin\frac{m\pi x}{l_*} \sin\frac{n\pi y}{h} \tag{24}$$

$$\Phi = \sum_{m=1}^{\infty}\sum_{n=1}^{\infty} B_{mn} \sin\frac{m\pi x}{l_*} \sin\frac{n\pi y}{h} \tag{25}$$

According to the Galerkin method and give $\eta = h/l_*$, Eqs. (24) and (25) can be simplified as Eqs. (26) and (27) respectively.

$$\begin{aligned} & A_{ij}\frac{D\pi^4}{4t\eta^3 l_*^2}\left(\eta^2 i^2 + j^2\right)^2 + \frac{\pi^2 l_3\left(l_1 + l_2\right)}{2\eta l_* l_1 l_2} j^2 \sin\frac{i\pi l_1}{l_*}\sum_{p=1}^{\infty} B_{pj}\sin\frac{p\pi l_1}{l_*} \\ & -8\tau\sum_{m=1}^{\infty}\sum_{n=1}^{\infty} A_{mn}\frac{mnij}{\left(i^2 - m^2\right)\left(j^2 - n^2\right)} = 0 \\ & (m \pm i = \text{odd},\ n \pm j = \text{odd}) \end{aligned} \tag{26}$$

$$B_{ij}\frac{\pi^4}{4E\eta^3 l_*^2}\left(\eta^2 i^2 + j^2\right)^2 - \frac{\pi^2 l_3\left(l_1 + l_2\right)}{2\eta l_* l_1 l_2} j^2 \sin\frac{i\pi l_1}{l_*}\sum_{m=1}^{\infty} A_{mj}\sin\frac{m\pi l_1}{l_*} = 0 \tag{27}$$

Make $\gamma = l_1/l_*$, then $l_1 = \gamma l_*$, $l_2 = \left(1-\gamma\right)l_*$, $l_3^2 = c^2 - \gamma^2 l_*^2$. By substituting Eq. (27) to Eq. (26), Eq. (26) can be simplified as Eq. (28).

$$\begin{aligned} & A_{ij}\frac{\pi^4}{4\eta^3}\frac{D}{tl_*^2}\left(\eta^2 i^2 + j^2\right)^2 \\ & +12\eta j^4(1-u^2)\frac{D}{tl_*^2}\frac{\left(c^2 - \gamma^2 l_*^2\right)}{t^2\gamma^2\left(1-\gamma\right)^2}\sin i\gamma\pi\sum_{p=1}^{\infty}\frac{\left(\sin p\gamma\pi\right)^2}{\left(\eta^2 p^2 + j^2\right)^2}\sum_{q=1}^{\infty} A_{qj}\sin q\gamma\pi \\ & -8\tau\sum_{m=1}^{\infty}\sum_{n=1}^{\infty} A_{mn}\frac{mnij}{\left(i^2 - m^2\right)\left(j^2 - n^2\right)} = 0 \\ & (m \pm i = \text{odd},\ n \pm j = \text{odd}) \end{aligned} \tag{28}$$

Table 2 shows that the flat panel width a is almost equal to the inclined panel width c for actual bridges with CSWs. Sayed-Ahmed [20] also proposed a=c. When a=c, then $l_1 = l_2 = 0.5 l_*$, $l_3 = a\sin\left(\theta/2\right)$. Eq. (28) can be simplified as Eq. (29).

$$\begin{aligned} & A_{ij}\frac{D}{tl_*^2}\frac{\pi^4}{4\eta^3}\left(\eta^2 i^2 + j^2\right)^2 \\ & +192\eta j^4(1-u^2)\sin\frac{i\pi}{2}\frac{D}{tl_*^2}\left(\frac{a}{t}\sin\frac{\theta}{2}\right)^2\sum_{p=1}^{\infty}\frac{\left(\sin\dfrac{p\pi}{2}\right)^2}{\left(\lambda^2 p^2 + j^2\right)^2}\sum_{q=1}^{\infty} A_{qj}\sin\frac{q\pi}{2} \\ & -8\tau\sum_{m=1}^{\infty}\sum_{n=1}^{\infty} A_{mn}\frac{mnij}{\left(i^2 - m^2\right)\left(j^2 - n^2\right)} = 0 \\ & (m \pm i = \text{odd},\ n \pm j = \text{odd}) \end{aligned} \tag{29}$$

By assigning values to i and j in Eq. (28) or (29), a series of linear algebraic equations with A_{mn} as unknowns can be obtained. Then the critical shear buckling stress can be derived by assuming the coefficient determinant of the linear algebraic equations equals zero. (i. e. a linear bifurcation analysis).

According to Eq. (28), the elastic interactive shear buckling stress of CSWs can be expressed as Eq. (30).

$$\tau_i^e = k_i \frac{D}{l_*^2 t} \tag{30}$$

For CSWs with a=c, Eq. (30) can be expressed as Eq. (31).

$$\tau_i^e = k_i \frac{Et^2}{12\left(1-\mu^2\right)\left(2a\cos\left(\theta/2\right)\right)^2} \tag{31}$$

where k_i is the elastic interactive shear buckling coefficient of CSWs. The detailed solution process of the coefficient k_i is given below.

2.4.2. Calculation of the interactive shear buckling coefficient k_i

According to Eq. (28) and using some mathematical softwares, the interactive shear buckling coefficient k_i can be calculated easily. According to Eq. (29), the coefficient k_i for CSWs with a=c is associated with the aspect ratio h/l_* and the parameter $\frac{a}{t}\sin\frac{\theta}{2}$.

Table 2 shows that the parameter a/t varies from 16 to 54. For CSWs used in actual bridges, values of θ between 30° and 45° are typical [31], so the parameter $\frac{a}{t}\sin\frac{\theta}{2}$ normally varies from 4 to 21. Table 8 shows the values of k_i in the case of $h/l_* \le 6$ and $0 \le \frac{a}{t}\sin\frac{\theta}{2} \le 30$. The coefficient k_i for CSWs with a=c can be calculated by linear interpolation.

Table 8
The interactive shear buckling coefficient of CSWs k_i

$a\sin(\theta/2)/t$ \ h/l	1	1.5	2	2.5	3	4	6
0	92.0294	69.7779	64.6068	59.5429	57.6401	55.5123	54.0737
0.25	93.1769	70.4358	65.1533	60.1504	58.2841	56.2034	54.7502
0.5	96.4737	72.3623	66.7412	61.6682	59.7653	57.7165	56.2556
0.75	101.5418	75.4292	69.2377	64.1539	62.2492	60.0918	58.6002
1	107.9047	79.4587	72.4772	67.3685	65.4597	63.3175	61.8178
1.25	115.1066	84.2573	76.3023	71.1993	69.2471	67.1066	65.6054
1.5	122.7766	89.6403	80.5822	75.4736	73.5211	71.3398	69.8362
1.75	130.6405	95.4438	85.2126	80.0664	78.1059	75.9049	74.4034
2	138.5077	101.529	90.1107	85.0094	83.0432	80.8299	79.3286
2.25	146.2490	107.7805	95.2084	90.1018	88.1264	85.8974	84.3952
2.5	153.7778	114.1043	100.4489	95.3454	93.3434	91.1428	89.6401
2.75	161.0361	120.4235	105.7836	100.2358	98.1972	96.0022	94.5007
3	167.9851	126.6760	111.1704	104.6219	102.5653	100.3454	98.6773
3.25	174.5993	132.8113	116.5728	109.0573	106.9074	104.6971	102.0138
3.5	180.8631	138.7891	121.9590	113.5325	110.5256	108.2896	105.3762
3.75	186.7687	144.5771	127.3010	118.0361	114.1704	111.9992	108.7868
4	192.3144	150.1502	132.5740	122.5558	117.8456	115.6795	112.2527
4.25	197.5036	155.4890	137.7565	127.0794	121.5508	119.3297	115.7745
4.5	202.3438	160.5796	142.8289	131.5948	125.2828	123.0553	119.3492
4.75	206.8458	165.4126	147.7743	136.0904	129.0371	126.7668	122.9721
5	211.0229	169.9825	152.5772	140.5553	132.8082	129.9071	126.6377
5.5	218.4650	178.3284	161.7019	149.3521	140.3772	135.0183	132.0734
6	224.8047	185.6367	170.1093	157.9097	147.9408	140.2147	137.4093
6.5	230.1828	191.9637	177.7254	166.1610	155.4507	145.4974	142.7003
7	234.7358	197.3909	184.4964	174.0451	162.8600	150.8560	148.1038
7.5	238.5894	202.0147	190.3940	181.5032	170.1220	156.2740	153.4890
8	241.8551	205.9366	195.4237	188.4706	177.1872	161.7319	159.0231
9	246.9941	212.0662	203.1006	197.9587	190.4379	172.6793	169.9498
10	249.6481	216.4745	208.2566	203.1951	196.9761	183.4995	178.9182
12	252.7794	222.0752	214.1494	209.0746	203.8849	193.4008	190.8814
14	254.6094	225.2856	217.2037	212.2282	208.4515	204.5305	202.8039
16	255.7683	227.2733	219.0022	214.6838	211.9712	209.8780	208.0037
18	256.5482	228.5854	220.1599	215.6484	212.9664	210.7748	209.0133
20	257.0984	229.4967	220.9213	216.3216	213.6575	211.4042	209.6595
22	257.5011	230.1558	221.4389	216.8106	214.1583	211.8635	210.0977
24	257.805	230.6483	221.8279	217.1773	214.5333	212.2091	210.4349
26	258.0399	231.0262	222.1278	217.4597	214.8217	212.4759	210.6952
28	258.2253	231.3226	222.3639	217.6818	215.0485	212.6861	210.9005
30	258.3743	231.5596	222.5532	217.8598	215.2300	212.8548	211.0652

2.5. Discussion of the local, global and interactive shear buckling stresses

Three shear buckling modes are discussed theoretically in this paper. Local buckling is the buckling of a panel and solved by analyzing a single flat panel under shear force, whereas global buckling is the buckling of the whole CSW and solved by treating the whole CSW as an orthotropic plate. Interactive buckling is the buckling of 2~4 panels and solved by treating the 2~4 panels as a folded plate.

Theoretically, the local shear buckling stress τ_l^e is associated with t/p, p/h which can be seen from Eqs. (4)-(7), whereas the global shear buckling stress τ_g^e is associated with θ, d/h and t/d which can be seen from Eqs. (17)-(20). The interactive shear buckling stress τ_i^e is associated with the geometric dimensioning of CSWs which can be seen from Eqs. (28)-(31). When CSWs have equal d/t, p/h and θ values, they will have an equal t/p ratio which affects the local shear buckling stress τ_l^e, and equal d/h and t/d ratios which affect the global shear buckling stress τ_g^e. In the case of a=c, they will have an equal $\eta = h/\left(2a\cos(\theta/2)\right)$ and $t/\left(a\cos(\theta/2)\right)$ which affect the interactive shear buckling stress τ_i^e. For CSWs with equal d/t, a/h and θ values, buckling stresses τ_l^e, τ_g^e, and τ_i^e will theoretically be equal.

3. Finite element analysis

An elastic FEA is carried out in the ANSYS software [32] to study the influence of d/t, a/h and θ on the shear buckling stress of CSWs and to see if the analytical formulas are correct. According to Yi et al. [15], a/h=0.1~0.2 and d/t=10~25 in actual bridges. In this study, conservatively adopting a/h=0.1~0.3 and d/t=10~30, while other geometric parameters are taken as: θ=30°~45° and t=8mm~12mm. The span of the girders is set as 20q. In addition, the width and the thickness of flanges are 8d and 80mm respectively. There are three stiffeners and their behavior is assumed to be rigid.

3.1. Finite element model

A shell element (shell 181) is used to model the girders with CSWs. The finite element model is shown in Fig. 6 and the boundary conditions are given in Table 9. A concentrated load is applied at the midspan (point 2). All models adopt a symmetry boundary condition with roller supports at the intersection nodes of the bottom flange and the end stiffeners, and Point 1 restrained in the longitudinal direction (x direction) [26]. In addition, Point 1 and Point 2 are restrained in the lateral direction (z direction) to avoid lateral-torsion buckling.

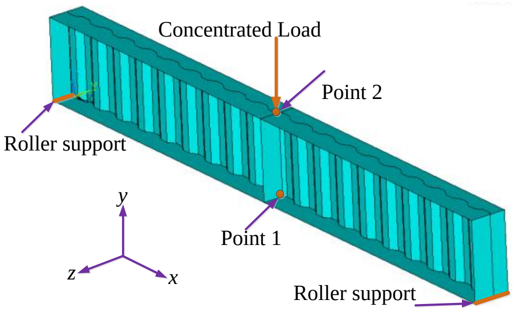

Fig. 6 Load and boundary conditions of a girder with CSWs

Table 9
Boundary conditions of finite element models

Boundary	δ_x	δ_y	δ_z	θ_x	θ_y	θ_z
Roller support	○	●	●	●	●	○
Point 1	●	○	●	○	○	○
Point 2	○	○	●	○	○	○

Note: ○: Free; ●: Restrained.

In this study, the number of elements per sub-panel is 6, as suggested by Eldib [3], and the element mesh size is a/6. The elastic modulus and Poisson's ratio of steel are taken as 210000MPa and 0.3 respectively. Fig. 7 represents three shear buckling modes of CSWs.

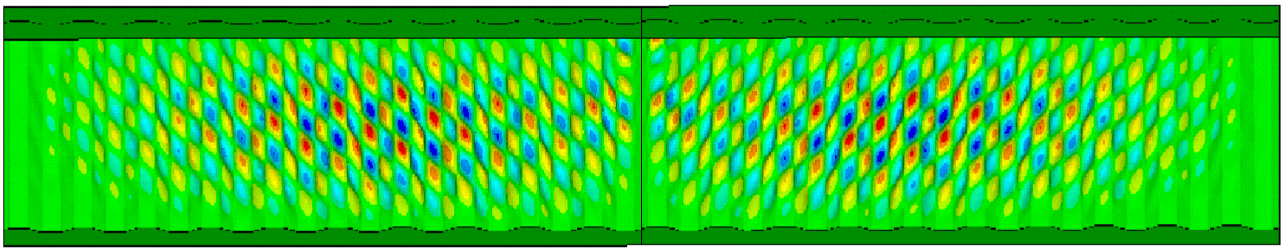

(a) Local shear buckling

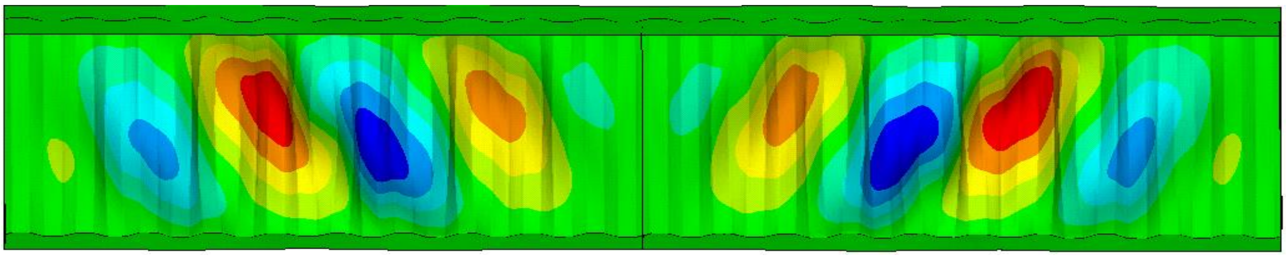

(b) Global shear buckling

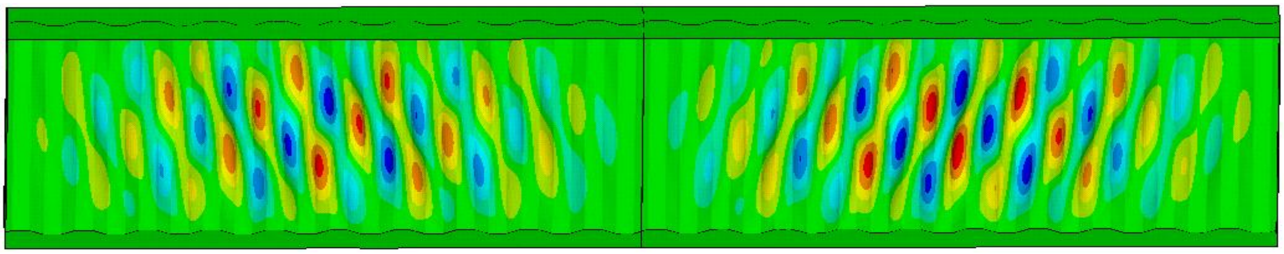

(c) Interactive shear buckling

Fig. 7 Three shear buckling modes

3.2. Parametric analysis

Theoretically, in the case of $a=c$, and equal d/t, a/h and θ, the elastic local shear buckling stress τ_l^e, global shear buckling stress τ_g^e, and interactive shear buckling stress τ_i^e should be equal. It can be seen from Fig. 8 that for CSWs with different web thicknesses but equal d/t, a/h and θ when $a=c$, the FEA results τ_{FEA}^e are indeed practically the equal which is in good agreement with the theoretical expectations. τ_{FEA}^e is the maximum shear stress of CSWs from FEA. It is worth mentioning that the d/t, a/h and θ are the determining factors, rather than t. In what follows, t=10mm is adopted.

The influence of d/t, a/h and θ on the elastic shear buckling stress is shown in Tables 10-12 and Figs. 9-10. It can be seen from Tables 10-12 and Figs. 9-10 that, apart from the global shear buckling modes with small d/t and small a/h, the FEA results agree well with the theoretical results τ_{cr}^e. The elastic shear buckling stress of CSWs τ_{cr}^e is controlled by the minimum value of local, global and interactive shear buckling stress, and can be calculated by Eq. (32).

$$\tau_{cr}^e = \text{minimum}\left(\tau_{l,s}^e, \tau_{g,s}^e, \tau_i^e\right) \tag{32}$$

It can be seen from Fig. 9 that the shear buckling stress greatly decreases with the increase of d/t. That is to say, improving the thickness of CSWs is an effective method to improve the shear buckling stress of CSWs. It can be seen from Fig. 10 (a) that the shear buckling stress increases with the increase of a/h. However, with the increase of a/h, the buckling stress τ_{FEA}^e shows a converging trend. It can be seen from Fig. 10 (b) that the shear buckling stress increases with the increase of θ. Though improving θ can improve the shear buckling stress, θ=30°~45° is adopted in actual engineering because larger θ need more steel and is not economic.

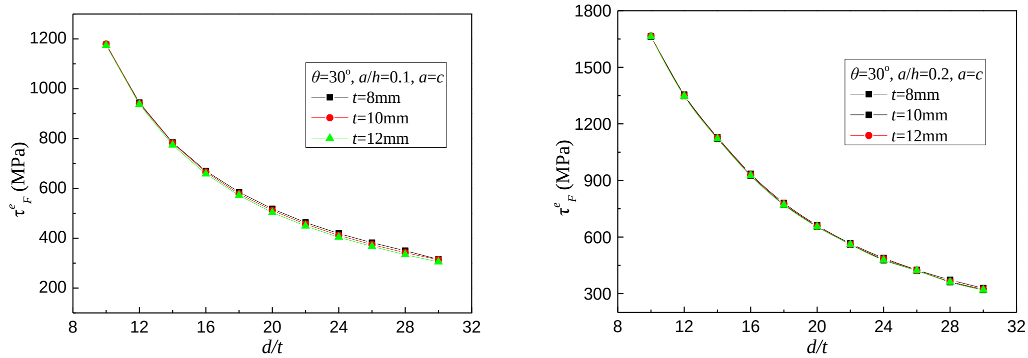

(a) a/h=0.1 (b) a/h=0.2

Fig. 8 Influence of t on the elastic shear buckling stress τ_{FEA}^e

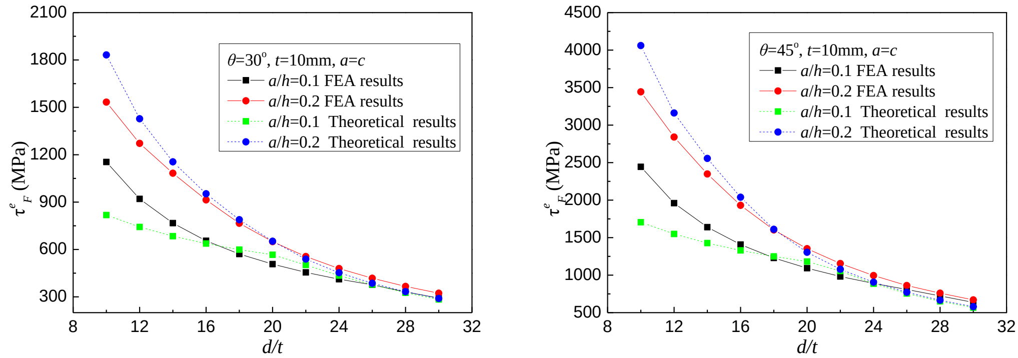

(a) θ=30° (b) θ=45°

Fig. 9 Influence of d/t on the elastic shear buckling stress

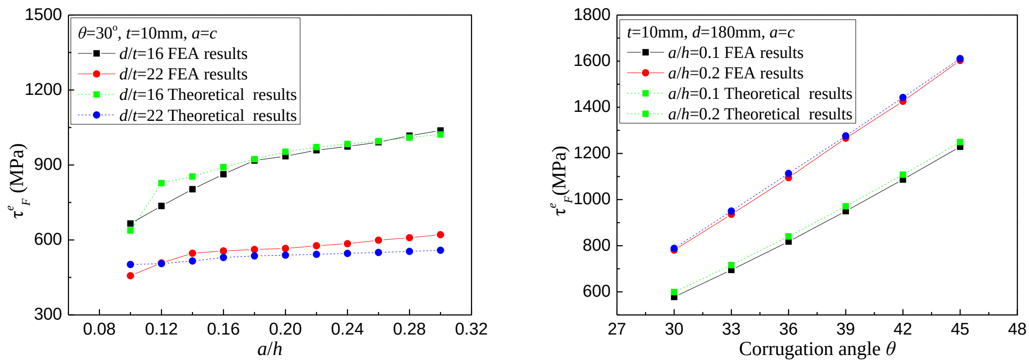

(a) a/h (b) θ

Fig. 10 Influence of a/h and θ on the elastic shear buckling stress

Table 10
Elastic shear buckling stress of CSWs with different *d*/*t*

θ (°)	a/h	d/t	a (mm)	b (mm)	d (mm)	h (mm)	$\tau_{l,s}$ (Mpa)	$\tau_{g,s}$ (Mpa)	τ_i (Mpa)	τ_{cr} (Mpa)	τ_{FEA} (Mpa)	τ_{FEA}/τ_{cr}^{e}	Buckling mode
		10	200	173	100	2000	2553	818	1673	818	1180	1.442	G
		12	240	208	120	2400	1773	743	1260	743	940	1.266	G
		14	280	242	140	2800	1302	684	998	684	782	1.142	G
		16	320	277	160	3200	997	638	821	638	665	1.043	G
		18	360	312	180	3600	788	599	692	599	578	0.965	G
	0.1	20	400	346	200	4000	638	567	589	567	511	0.903	G
		22	440	381	220	4400	527	539	502	502	457	0.910	I
		24	480	416	240	4800	443	514	435	435	412	0.947	I
		26	520	450	260	5200	378	493	382	378	374	0.991	L
		28	560	485	280	5600	326	474	337	326	342	1.050	L
30		30	600	520	300	6000	284	457	297	284	314	1.105	L
		10	200	173	100	1000	2610	3272	1832	1832	1664	0.908	I
		12	240	208	120	1200	1812	2971	1428	1428	1354	0.949	I
		14	280	242	140	1400	1332	2738	1155	1155	1129	0.977	I
		16	320	277	160	1600	1019	2551	953	953	935	0.981	I
		18	360	312	180	1800	805	2396	789	789	781	0.990	I
	0.2	20	400	346	200	2000	652	2266	654	652	662	1.015	L
		22	440	381	220	2200	539	2155	549	539	566	1.050	L
		24	480	416	240	2400	453	2058	467	453	489	1.079	L
		26	520	450	260	2600	386	1972	401	386	426	1.103	L
		28	560	485	280	2800	333	1897	349	333	373	1.121	L
		30	600	520	300	3000	290	1828	306	290	329	1.135	L
		10	141	100	100	1414	5106	1706	3717	1706	2444	1.433	G
		12	170	120	120	1697	3546	1549	2806	1549	1960	1.266	G
		14	198	140	140	1980	2605	1427	2229	1427	1640	1.149	G
		16	226	160	160	2263	1994	1330	1837	1330	1408	1.059	G
	0.1	18	255	180	180	2546	1576	1249	1546	1249	1229	0.984	G
		20	283	200	200	2828	1276	1182	1302	1182	1093	0.925	G
		22	311	220	220	3111	1055	1124	1112	1055	982	0.931	L
		24	339	240	240	3394	886	1073	965	886	890	1.004	L
		26	368	260	260	3677	755	1028	848	755	809	1.071	L
		28	396	280	280	3960	651	989	741	651	723	1.110	L
45		30	424	300	300	4243	567	953	653	567	637	1.123	L
		10	141	100	100	707	5220	6823	4061	4061	3444	0.848	I
		12	170	120	120	849	3625	6195	3162	3162	2841	0.899	I
		14	198	140	140	990	2663	5709	2556	2556	2349	0.919	I
		16	226	160	160	1131	2039	5320	2102	2039	1931	0.947	L
		18	255	180	180	1273	1611	4998	1731	1611	1603	0.995	L
	0.2	20	283	200	200	1414	1305	4727	1431	1305	1353	1.037	L
		22	311	220	220	1556	1078	4494	1202	1078	1155	1.071	L
		24	339	240	240	1697	906	4292	1021	906	995	1.098	L
		26	368	260	260	1838	772	4114	878	772	862	1.116	L
		28	396	280	280	1980	666	3955	763	666	760	1.142	L
		30	424	300	300	2121	580	3813	669	580	670	1.155	L
Average												1.054	
Coefficient of variation												0.122	
Average (G)												1.131	
Coefficient of variation (G)												0.165	
Average (I and L)												1.024	
Coefficient of variation (I and L)												0.083	

Table 11
Elastic shear buckling stress of CSWs with different *a*/*h*

θ (°)	*d*/*t*	*a*/*h*	*a* (mm)	*b* (mm)	*d* (mm)	*h* (mm)	$\tau_{l,s}$ (Mpa)	$\tau_{g,s}$ (Mpa)	τ_i (Mpa)	τ_{cr} (Mpa)	τ_{FEA} (Mpa)	τ_{FEA}/τ_{cr}^e	Buckling mode
		0.1	320	277	160	3200	997	638	821	638	665	1.043	G
		0.12	320	277	160	2667	1000	918	827	827	736	0.890	I
		0.14	320	277	160	2286	1004	1250	854	854	803	0.940	I
		0.16	320	277	160	2000	1009	1632	891	891	863	0.968	I
		0.18	320	277	160	1778	1014	2066	923	923	918	0.994	I
	16	0.2	320	277	160	1600	1019	2551	953	953	935	0.981	I
		0.22	320	277	160	1455	1026	3086	971	971	959	0.987	I
		0.24	320	277	160	1333	1032	3673	984	984	974	0.990	I
		0.26	320	277	160	1231	1040	4311	995	995	991	0.996	I
		0.28	320	277	160	1143	1048	4999	1010	1010	1017	1.007	I
30		0.3	320	277	160	1067	1057	5739	1022	1022	1038	1.016	I
		0.1	440	381	220	4400	527	539	502	502	457	0.911	I
		0.12	440	381	220	3667	529	776	505	505	508	1.005	I
		0.14	440	381	220	3143	531	1056	516	516	547	1.060	I
		0.16	440	381	220	2750	534	1379	530	530	556	1.049	I
		0.18	440	381	220	2444	536	1745	541	536	562	1.048	L
	22	0.2	440	381	220	2200	539	2155	549	539	566	1.050	L
		0.22	440	381	220	2000	542	2607	556	542	577	1.064	L
		0.24	440	381	220	1833	546	3103	561	546	585	1.071	L
		0.26	440	381	220	1692	550	3642	566	550	599	1.089	L
		0.28	440	381	220	1571	554	4224	572	554	609	1.099	L
Average												1.012	
Coefficient of variation												0.055	

Table 12
Elastic shear buckling stress of CSWs with different θ

d/*t*	*a*/*h*	θ (°)	*a* (mm)	*b* (mm)	*d* (mm)	*h* (mm)	$\tau_{l,s}$ (Mpa)	$\tau_{g,s}$ (Mpa)	τ_i (Mpa)	τ_{cr} (Mpa)	τ_{FEA} (Mpa)	τ_{FEA}/τ_{cr}^e	Buckling mode
		30	360	312	360	3600	788	599	692	599	578	0.965	G
		33	330	277	330	3305	935	716	824	716	695	0.971	G
	0.1	36	306	248	306	3062	1089	840	964	840	818	0.974	G
		39	286	222	286	2860	1248	971	1110	971	950	0.978	G
		42	269	200	269	2690	1411	1108	1260	1108	1087	0.981	G
18		45	255	180	255	2546	1576	1249	1414	1249	1229	0.984	G
		30	360	312	360	1800	805	2396	789	789	781	0.990	I
		33	330	277	330	1652	956	2863	950	950	936	0.985	I
	0.2	36	306	248	306	1531	1113	3361	1126	1113	1095	0.984	L
		39	286	222	286	1430	1276	3885	1315	1276	1266	0.992	L
		42	269	200	269	1345	1443	4432	1516	1443	1426	0.989	L
		45	255	180	255	1273	1611	4998	1729	1611	1603	0.995	L
Average												0.982	
Coefficient of variation												0.009	

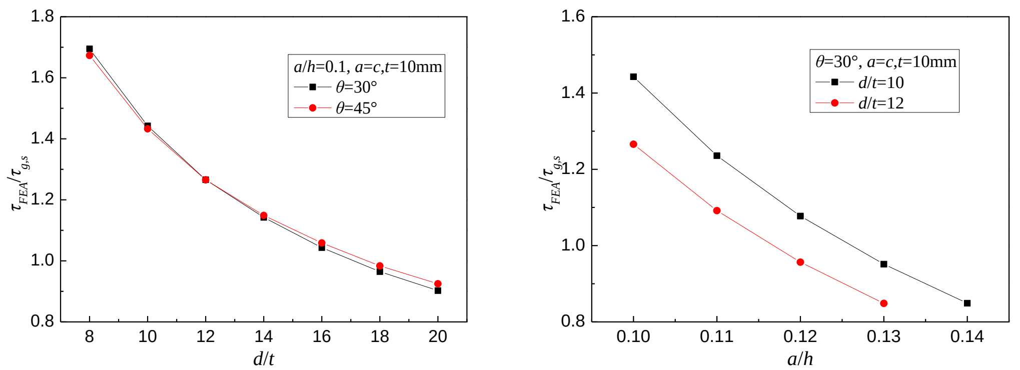

(a) *d*/*t* (b) *a*/*h*

Fig. 11 Influence of *d*/*t* and *a*/*h* on $\tau_{FEA}^e/\tau_{g,s}^e$

The boundary condition of the global buckling mode is complicated. Fig. 11 shows the ratios of τ_{FEA}^e to $\tau_{g,s}^e$ varies with *d*/*t* and *a*/*h* in the case of $\tau_{g,s}^e < minimum\left(\tau_{l,s}^e, \tau_i^e\right)$ which the global buckling becomes the primary failure mode. It can be seen from Fig. 11 that $\tau_{FEA}^e/\tau_{g,s}^e$ decreases with the increase of *d*/*t* and *a*/*h*. That is to say, the constraint effect of flanges on CSWs gradually decreases with the increase of *d*/*t* and *a*/*h*. Although the ratios of τ_{FEA}^e to $\tau_{g,s}^e$ are high for small *d*/*t* and *a*/*h*, the simple support boundary condition is adopted for conservative consideration.

4. Shear design of CSWs

Considering material nonlinearity and yielding, the formula for the elastic shear buckling stress cannot keep up with the actual. So a formula which can reflect the actual shear strength needs to be proposed. Important work has been done by Elgaaly [22], Driver [23], El Metwally [17], Yi et al. [15], Sause [31], Nie et al.[21]. The previous design formulas may be not precise because adopting the interactive shear buckling stress formula which based on the relationship between the local and global shear buckling stresses, and the yield stress only. All the previous elastic interactive formulas adopt $\left(1/\tau_i^e\right)^n=\left(1/\tau_l^e\right)^n+\left(1/\tau_g^e\right)^n$, n=1~4 [15], show that the interactive shear buckling stress is the minimum value of the three shear buckling modes, which is not reasonable and lacks theoretical support. Unlike the past, in this study, the formulas for the elastic global and interactive shear buckling stresses proposed in section 2 are used in the design formula.

Eq. (33) was provided to calculate the ultimate shear strength of CSWs in the design manual for PC bridges with CSWs [33].

$$\tau_{cr}=\tau_y\times\begin{cases}1 & \lambda_{cr}\le 0.6\\ 1-0.614\left(\lambda_{cr}-0.6\right) & 0.6\le\lambda_{cr}\le\sqrt{2}\\ 1/\lambda_{cr}^2 & \lambda_{cr}>\sqrt{2}\end{cases} \tag{33}$$

$$\lambda_{cr}=\sqrt{\tau_y/\tau_{cr}^{e*}} \tag{34}$$

For conservative consideration, τ_{cr}^{e*} adopts Eq. (32) introducing a modification factor.

$$\tau_{cr}^{e*}=\text{minimum}\left(0.85\tau_{l,s}^e,\tau_{g,s}^e,0.85\tau_i^e\right) \tag{35}$$

where τ_y is the shear yield stress and can be calculated by $\tau_y=f_y/\sqrt{3}$, f_y is the uniaxial yield stress.

Eq. (33) is verified by using published experimental results of 102 specimens obtained by Elgaaly et al. [22], Lindner et al. [34], Peil [35], Gil et al. [36], Abbas et al. [18], Moon et al.[24]. Tables 13-18 show a comparison between the shear strength calculated by Eq. (33) and four previous design methods and experimental results τ_e [31]. In Tables 13-18, $\tau_{n,A}$, $\tau_{n,B}$, $\tau_{n,M}$, $\tau_{n,Y}$ are the shear strength of CSWs calculated by the four previous design methods proposed by Driver [23], Sause [31], El Metwally [17], Yi et al. [15]. Fig. 12 shows the normalized shear capacity τ_e/τ_y and τ_e/τ_{cr} versus λ_{cr} . It can be seen that all the tests have a ratio $\tau_e/\tau_{cr}\ge 0.8$.

Table 13

Comparison between the shear strength calculated by the proposed design formulas and the test results obtained by Elgaaly et al.[22]

Specimen	e/h	a (mm)	b (mm)	θ (°)	h (mm)	t (mm)	τ_y (Mpa)	τ_e (Mpa)	λ_{cr}	τ_{cr} (Mpa)	τ_e/τ_{cr}	$\tau_e/\tau_{n,A}$	$\tau_e/\tau_{n,B}$	$\tau_e/\tau_{n,M}$	$\tau_e/\tau_{n,Y}$
V-PILOTA	1	38.1	25.4	45	304.8	0.7823	358	346.54	1.03	262.5	1.320	1.404	1.349	1.316	1.363
V-PILOTB	1	38.1	25.4	45	304.8	0.7849	368	347.54	1.05	267.4	1.300	1.177	1.132	1.109	1.149
V121216A	1	38.1	25.4	45	304.8	0.6375	389.8	257.3	1.32	216.4	1.189	1.159	1.132	1.178	1.194
V121216B	1	38.1	25.4	45	304.8	0.7645	383.8	375.8	1.10	267.0	1.408	1.464	1.41	1.405	1.452
V181216B	0.67	38.1	25.4	45	457.2	0.6096	356.8	334.9	1.33	197.0	1.700	1.649	1.64	1.768	1.993
V181216C	0.67	38.1	25.4	45	457.2	0.7595	391.5	343.9	1.12	267.1	1.288	1.325	1.316	1.385	1.539
V181816A	1	38.1	25.4	45	457.2	0.635	341.3	257.2	1.25	205.5	1.252	1.22	1.228	1.311	1.449
V181816B	1	38.1	25.4	45	457.2	0.7366	354.2	285.4	1.10	246.3	1.159	1.203	1.185	1.232	1.359
V241216A	0.5	38.1	25.4	45	609.6	0.635	341.3	195.1	1.25	205.2	0.951	0.996	1.01	1.129	1.374
V241216B	0.5	38.1	25.4	45	609.6	0.7874	339.2	277.7	1.03	250.1	1.110	1.238	1.252	1.343	1.523
V121221A	1	41.9	23.4	55	304.8	0.6299	383.8	240.8	1.46	179.8	1.339	1.27	1.226	1.277	1.236
V121221B	1	41.9	23.4	55	304.8	0.7849	383.8	302.9	1.17	248.9	1.217	1.227	1.194	1.202	1.189
V122421A	2	41.9	23.4	55	304.8	0.6756	358	210	1.32	200.7	1.046	1.023	0.998	1.028	0.996
V122421B	2	41.9	23.4	55	304.8	0.7823	368	256.5	1.15	243.3	1.054	1.073	1.04	1.041	1.031
V181221A	0.67	41.9	23.4	55	457.2	0.6096	333.4	221.7	1.41	167.1	1.327	1.274	1.236	1.302	1.356
V181221B	0.67	41.9	23.4	55	457.2	0.762	349.6	280.7	1.16	230.0	1.220	1.236	1.204	1.23	1.29
V181821A	1	41.9	23.4	55	457.2	0.635	318.3	194.4	1.32	176.6	1.101	1.07	1.046	1.095	1.13
V181821B	1	41.9	23.4	55	457.2	0.7366	343.9	277.2	1.19	219.9	1.260	1.26	1.234	1.268	1.326
V241221A	0.5	41.9	23.4	55	609.6	0.6096	351.7	207.8	1.45	166.7	1.247	1.177	1.159	1.26	1.468
V241221B	0.5	41.9	23.4	55	609.6	0.762	368.5	272.6	1.19	235.1	1.159	1.157	1.165	1.248	1.399
V121232A	1	49.8	26.4	62.5	304.8	0.6401	383.8	210.8	1.70	132.2	1.594	1.83	1.781	1.831	1.803
V121232B	1	49.8	26.4	62.5	304.8	0.7798	369.9	257.1	1.37	194.4	1.323	1.594	1.536	1.596	1.499
V121832A	1.5	49.8	26.4	62.5	304.8	0.6401	405.8	176.6	1.75	132.2	1.336	1.526	1.488	1.526	1.511
V121832B	1.5	49.8	26.4	62.5	304.8	0.9195	324.2	190.3	1.09	226.7	0.840	0.963	0.947	0.964	0.906
V122432A	2	49.8	26.4	62.5	304.8	0.6401	411.8	159.5	1.76	132.2	1.206	1.376	1.343	1.377	1.365
V122432B	2	49.8	26.4	62.5	304.8	0.7772	366	206.4	1.37	192.9	1.070	1.289	1.242	1.29	1.211
V181232A	0.67	49.8	26.4	62.5	457.2	0.5969	318.2	188.9	1.67	113.7	1.661	1.895	1.842	1.899	1.921
V181232B	0.67	49.8	26.4	62.5	457.2	0.7493	347.5	233.6	1.39	178.4	1.309	1.563	1.507	1.569	1.545
V181832A	1	49.8	26.4	62.5	457.2	0.6096	397.8	189.8	1.83	118.6	1.600	1.797	1.757	1.801	1.854
V181832B	1	49.8	26.4	62.5	457.2	0.7493	334.6	229.4	1.37	177.2	1.295	1.547	1.49	1.552	1.518
V241232A	0.5	49.8	26.4	62.5	609.6	0.6223	388.5	182	1.78	123.1	1.478	1.662	1.622	1.674	1.798
V241232B	0.5	49.8	26.4	62.5	609.6	0.762	337.1	218.3	1.35	181.6	1.202	1.43	1.38	1.447	1.496
V121809A	1.5	19.8	11.9	50	304.8	0.7061	330.2	293.3	0.79	291.1	1.007	1.256	1.163	1.066	1.119
V121809C	1.5	19.8	11.9	50	304.8	0.6325	385.8	285.9	0.88	318.9	0.896	1.048	1.003	0.97	1.04
V122409A	2	19.8	11.9	50	304.8	0.7137	338.1	265.6	0.80	296.6	0.895	1.111	1.03	0.947	0.994
V122409C	2	19.8	11.9	50	304.8	0.6629	358	286	0.84	305.4	0.937	1.13	1.062	1.001	1.063
V181209A	0.67	19.8	11.9	50	457.2	0.5588	397.8	316.7	1.39	205.2	1.544	1.672	1.621	1.722	1.883
V181209C	0.67	19.8	11.9	50	457.2	0.6096	341.6	318.3	1.26	203.7	1.563	1.694	1.65	1.73	1.779
V181809A	1	19.8	11.9	50	457.2	0.6096	356.7	295	1.28	206.7	1.427	1.551	1.507	1.584	1.637
V181809C	1	19.8	11.9	50	457.2	0.6223	322.4	272.6	1.21	200.7	1.358	1.468	1.436	1.495	1.525
V241209A	0.5	19.8	11.9	50	609.6	0.6223	349.6	186.4	1.69	122.9	1.517	1.553	1.505	1.565	1.654
V241209C	0.5	19.8	11.9	50	609.6	0.635	358	204.8	1.70	124.2	1.649	1.686	1.635	1.698	1.792
Average											1.270	1.363	1.326	1.367	1.422
Coefficient of variation (C.V.)											0.175	0.182	0.182	0.194	0.198

Table 14
Comparison between the shear strength calculated by the proposed design formulas and the test results obtained by Lindner et al. [34]

Specimen	e/h	a (mm)	b (mm)	θ (°)	h (mm)	t (mm)	τ_y (Mpa)	τ_e (Mpa)	λ_{cr}	τ_{cr} (Mpa)	τ_e/τ_{cr}	$\tau_e/\tau_{n,A}$	$\tau_e/\tau_{n,B}$	$\tau_e/\tau_{n,M}$	$\tau_e/\tau_{n,Y}$
L1A	0.98	140	50	45	994	1.94	169	145.5	1.00	127.1	1.144	1.259	1.210	1.190	1.235
L1B	0.99	140	50	45	994	2.59	193	194.5	0.80	168.9	1.152	1.426	1.316	1.202	1.266
L2A	1.04	140	50	45	1445	1.94	163	120.3	0.99	124.1	0.970	1.069	1.050	1.072	1.178
L2B	1.04	140	50	45	1445	2.54	183	153.7	0.80	160.5	0.958	1.187	1.120	1.080	1.180
L3A	1	140	50	45	2005	2.01	162	111.9	1.07	115.7	0.967	1.065	1.080	1.165	1.324
L3B	1	140	50	45	2005	2.53	173	152.6	1.04	126.7	1.204	1.338	1.312	1.361	1.484
B1	1.33	140	50	45	600	2.1	197	165.1	0.99	150.0	1.100	1.225	1.174	1.136	1.122
B4	1.33	140	50	45	600	2.11	210	144.9	1.02	156.4	0.926	1.022	0.981	0.958	0.944
B4b	1.33	140	50	45	600	2.11	210	171.8	1.02	156.4	1.098	1.212	1.163	1.136	1.120
B3	1.33	140	50	45	600	2.62	183	156.5	0.76	164.6	0.950	1.209	1.105	0.976	0.974
B2	1.17	140	50	45	600	2.62	182	173.8	0.76	164.0	1.060	1.350	1.234	1.088	1.086
M101	1	70	15	45	600	0.99	109	89.2	0.79	96.2	0.927	1.156	1.086	1.039	1.133
M102	1	70	15	45	800	0.99	110	100.0	1.00	83.0	1.205	1.354	1.326	1.370	1.500
M103	1	70	15	45	1000	0.95	123	88.4	1.34	67.4	1.313	1.443	1.413	1.526	1.748
M104	1	70	15	45	1200	0.99	109	87.4	1.49	48.9	1.789	1.922	1.862	1.975	2.200
L1	1.5	106	86.6	30	1000	2.1	237	181.1	0.83	203.0	0.892	1.081	1.013	0.962	1.039
L1	1.49	106	86.6	30	1000	3	260	203.6	0.65	251.3	0.810	1.107	1.003	0.884	0.931
L2	1.44	106	86.6	30	1498	2	217	200.3	0.98	166.5	1.203	1.354	1.336	1.384	1.531
L2	1.43	106	86.6	30	1498	3	232	201.4	0.91	188.0	1.071	1.229	1.186	1.145	1.201
No.1	1.33	102	85.5	33	850	2	205	161.7	0.78	182.0	0.889	1.116	1.024	0.921	0.960
No.2	1.33	91	71.5	38.2	850	2	201	155.6	0.69	189.6	0.820	1.094	0.990	0.861	0.890
V1/1	9.46	144	102	45	298	2.05	172	111.3	0.92	138.7	0.803	0.938	0.899	0.863	0.821
V1/2	6.71	144	102	45	298	2.1	163	111.7	0.87	136.0	0.821	0.968	0.930	0.876	0.838
V1/3	3.36	144	102	45	298	2	172	135.9	0.94	136.2	0.997	1.161	1.113	1.077	1.020
V2/3	2.75	144	102	45	600	3	161	130.4	0.64	156.8	0.832	1.146	1.031	0.869	0.833
Average											1.036	1.217	1.158	1.125	1.182
C.V.											0.206	0.164	0.173	0.225	0.269

Table 15
Comparison between the shear strength calculated by the proposed design formulas and the test results obtained by Gil et al. [36]

Specimen	e/h	a (mm)	b (mm)	θ (°)	h (mm)	t (mm)	τ_y (Mpa)	τ_e (Mpa)	λ_{cr}	τ_{cr} (Mpa)	τ_e/τ_{cr}	$\tau_e/\tau_{n,A}$	$\tau_e/\tau_{n,B}$	$\tau_e/\tau_{n,M}$	$\tau_e/\tau_{n,Y}$
L1	NA	450	300	33.7	1500	4.8	144.3	103.8	1.174	93.4	1.111	1.188	1.167	1.188	1.103
L2	NA	550	300	32.2	1500	4.8	144.3	87	1.413	72.2	1.205	1.328	1.280	1.328	1.214
L3	NA	450	300	9.4	1500	4.8	144.3	74	1.192	91.9	0.806	0.847	0.836	0.870	0.905
L4	NA	550	300	10.6	1500	4.8	144.3	66	1.413	72.2	0.914	1.007	0.972	1.018	1.043
G1	NA	200	180	14.2	2000	4.8	144.3	114.4	0.917	116.2	0.985	1.133	1.090	1.053	1.092
G2	NA	160	50	33.4	2000	3.8	144.3	120.4	1.143	96.2	1.252	1.366	1.346	1.384	1.388
G3	NA	160	100	15.1	2000	3.8	144.3	122.7	1.391	74.2	1.653	1.852	1.786	1.866	1.871
I1	NA	320	100	24.0	2000	4.8	144.3	137.1	0.862	121.1	1.132	1.343	1.321	1.338	1.480
I2	NA	350	100	16.0	2000	3.8	144.3	74.6	1.265	85.4	0.874	1.054	1.038	1.174	1.481
Average											1.103	1.235	1.204	1.247	1.286
C.V.											0.233	0.234	0.229	0.230	0.231

Note: NA-Not available

Table 16
Comparison between the shear strength calculated by the proposed design formulas and the test results ob-tained by Peil [35]

Specimen	e/h	a (mm)	b (mm)	θ (°)	h (mm)	t (mm)	τ_y (Mpa)	τ_e (Mpa)	λ_{cr}	τ_{cr} (Mpa)	τ_e/τ_{cr}	$\tau_e/\tau_{n,A}$	$\tau_e/\tau_{n,B}$	$\tau_e/\tau_{n,M}$	$\tau_e/\tau_{n,Y}$
SP1	2.19	146	104	45	800	2	177	140.7	1.03	129.9	1.083	1.189	1.143	1.120	1.080
SP2	2.19	170	80	45	800	2	172	134.3	1.18	110.6	1.214	1.274	1.254	1.277	1.209
SP3	2.19	185	65	45	800	2	168	130.7	1.27	99.2	1.317	1.397	1.358	1.400	1.322
SP4	2.25	117	83	45	800	2	172	144.5	0.82	148.8	0.971	1.188	1.097	0.988	0.986
SP5	2.25	136	64	45	800	2	168	138.1	0.94	133.0	1.038	1.163	1.118	1.059	1.059
SP6	2.25	148	52	45	800	2	169	137.1	1.02	125.1	1.096	1.204	1.156	1.134	1.135
SP2-2-400 1	2.5	170	80	45	400	2	152	100.6	1.06	109.1	0.922	1.029	1.001	1.001	0.934
SP2-2-400 2	2.5	170	80	45	400	2	152	110.5	1.06	109.1	1.013	1.130	1.099	1.099	1.026
SP2-2-800 1	1.25	170	80	45	800	2	157	111.8	1.13	106.0	1.054	1.119	1.094	1.100	1.049
SP2-2-800 2	1.25	170	80	45	800	2	157	111.0	1.13	106.0	1.047	1.112	1.087	1.093	1.042
SP2-3-600 1	1.67	170	80	45	600	3	170	167.8	0.77	151.9	1.104	1.396	1.280	1.134	1.109
SP2-3-600 2	1.67	170	80	45	600	3	170	171.7	0.77	151.9	1.130	1.429	1.310	1.161	1.135
SP2-3-1200 1	0.83	170	80	45	1200	3	170	170.0	0.79	150.2	1.132	1.415	1.298	1.161	1.188
SP2-3-1200 2	0.83	170	80	45	1200	3	170	173.9	0.79	150.2	1.158	1.447	1.327	1.188	1.215
SP2-4-800 1	1.25	170	80	45	800	4	188	188.0	0.62	186.0	1.011	1.415	1.269	1.063	1.033
SP2-4-800 2	1.25	170	80	45	800	4	188	188.6	0.62	186.0	1.014	1.419	1.273	1.066	1.036
SP2-4-1600 1	0.63	170	80	45	1600	4	189	189.6	0.63	185.9	1.020	1.418	1.278	1.104	1.147
SP2-4-1600 2	0.63	170	80	45	1600	4	189	191.3	0.63	185.9	1.029	1.432	1.290	1.114	1.158
SP2-8-800 1	1.25	170	80	45	800	8	156	205.0	0.28	156.0	1.314	1.858	1.656	1.319	1.314
SP2-8-800 2	1.25	170	80	45	800	8	156	215.4	0.28	156.0	1.381	1.952	1.739	1.385	1.381
Average											1.102	1.349	1.256	1.148	1.128
C.V.											0.110	0.173	0.145	0.100	0.104

Table 17

Comparison between the shear strength calculated by the proposed design formulas and the test results ob-tained by Abbas et al.[18]

Specimen	e/h	a (mm)	b (mm)	θ (°)	h (mm)	t (mm)	τ_y (Mpa)	τ_e (Mpa)	λ_{cr}	τ_{cr} (Mpa)	τ_e/τ_{cr}	$\tau_e/\tau_{n,A}$	$\tau_e/\tau_{n,B}$	$\tau_e/\tau_{n,M}$	$\tau_e/\tau_{n,Y}$
G8A	3	300	200	36.9	1500	6.3	268	228.6	0.88	221.9	1.030	1.207	1.12	1.017	1.023
G7A	3	300	200	36.9	1500	6.3	268	243.1	0.88	221.9	1.095	1.282	1.188	1.077	1.084
SC1	3	300	200	36.9	1500	6.3	268	213.3	0.88	221.9	0.961	1.126	1.045	0.949	0.955
Average											1.029	1.205	1.118	1.014	1.021
C.V.											0.065	0.065	0.064	0.063	0.063

Table 18.

Comparison between the shear strength calculated by the proposed design formulas and the test results obtained by Moon et al. [24]

Specimen	e/h	a (mm)	b (mm)	θ (°)	h (mm)	t (mm)	τ_y (Mpa)	τ_e (Mpa)	λ_{cr}	τ_{cr} (Mpa)	τ_e/τ_{cr}	$\tau_e/\tau_{n,A}$	$\tau_e/\tau_{n,B}$	$\tau_e/\tau_{n,M}$	$\tau_e/\tau_{n,Y}$
MI2	0.803	250	220	17.2	2000	4	170.9	109.2	0.93	136.1	0.803	0.904	0.889	0.9	0.996
MI3	0.728	220	180	14.6	2000	4	170.9	105.4	1.01	127.6	0.826	0.872	0.837	0.822	0.899
MI4	0.887	220	180	18.7	2000	4	170.9	131.6	0.84	146.2	0.900	1.089	1.013	0.955	1.036
Average											0.843	0.955	0.913	0.892	0.977
C.V.											0.061	0.123	0.099	0.075	0.072

Table 19

Comparison between test results and theoretical results

Specimen	Num.	τ_e/τ_{cr}		$\tau_e/\tau_{n,A}$		$\tau_e/\tau_{n,B}$		$\tau_e/\tau_{n,M}$		$\tau_e/\tau_{n,Y}$	
		Mean	C.V.	Mean	C.V.	Mean	C.V.	Mean	C.V.	Mean	C.V.
All	102	1.146	0.199	1.297	0.188	1.242	0.187	1.230	0.214	1.269	0.231
e/h>1 and $\theta\geq 30°$	46	1.028	0.138	1.221	0.165	1.151	0.151	1.086	0.145	1.083	0.148

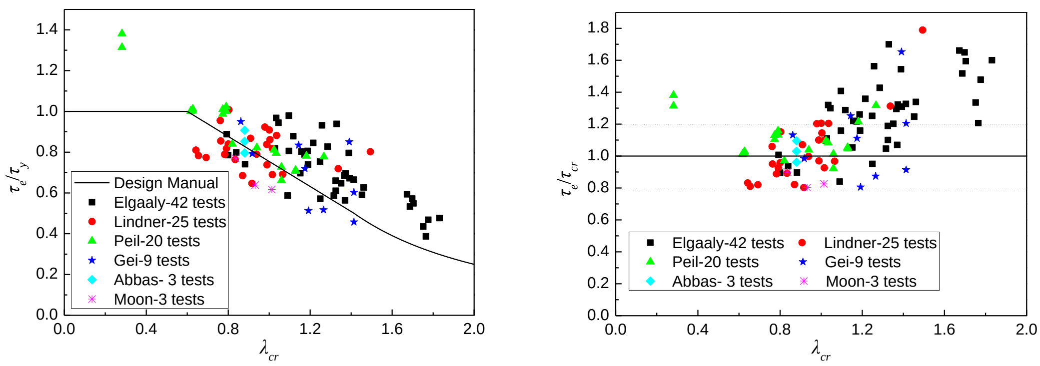

(a) τ_e/τ_y *versus* λ_{cr} (b) τ_e/τ_{cr} *versus* λ_{cr}

Fig. 12 Comparison between the shear strength calculated by Eq. (33) and the test results

For actual bridges, the distance between two adjacent stiffeners is much larger than the web height h, and θ always meets $\theta\geq 30°$[37], so the experimental results for the 46 specimens with e/h>1 and $\theta\geq 30°$ are selected. e/h is the shear span ratio[31]. The comparison between test results and theoretical results is given in Table 19. It can be seen that Eq. (33) which adopts the formulas for the elastic global and interactive shear buckling stresses proposed in this study provides on average much more accurate predictions of the shear strength of CSWs for the 102 specimens, and provides much more accurate predictions with the best average value and smallest coefficient of variation for the 46 specimens. So Eq. (33) is recommended to calculate the shear strength of CSWs.

It is worth mentioning that in Table 18, Reference [31] adopted the design corrugation depth of CSWs, however according to Reference [24], the negative error between the design corrugation depth and the measured corrugation depth can reach to 20%. Because the buckling will initiate at the area that has the minimum measured corrugation depth [24], the minimum measured corrugation depth is adopted in this paper.

5. Conclusions

In this paper, the shear capacity of CSWs is theoretically and numerically studied, and the following main conclusions can be drawn:

(1) The whole CSW is assumed as an orthotropic plate, and the analytical formula for the global shear buckling stress of CSWs is derived by the Galerkin method. Simplified formulas of the global shear buckling coefficient k_g for a four-edge simple support, for a four-edge fixed support, and for two edges constrained by flanges fixed and the other two edges simply supported are given.

(2) The folded plate composed of two adjacent panels is treated as an isotropic shallow shell, and the analytical formula for the interactive shear buckling stress of CSWs is derived by the Galerkin method. The interactive shear buckling coefficient table for CSWs with the same flat panel and inclined panel width is given.

(3) An elastic FEA is carried out to verify the analytical formulas and to study the influence of geometric parameters on the shear buckling stress of CSWs. Results show that the shear buckling stress greatly decreases with the increase of d/t, while increases with the increase of a/h and θ.

(4) A design formula for the shear strength of CSWs which adopts the formulas for the global and interactive shear buckling stresses proposed in this paper is assessed. From a comparison between the shear strength calculated by this design formula, calculated by four previous design formulas and measured in a series of published test results, it is found that the considered design formula provides good predictions for the shear strength of CSWs and can be recommended.

Acknowledgments

The supports from the National Natural Science Foundation of China (grant no.51378106) and the China Scholarship Council are gratefully acknowledged.

References

[1] Hamilton R.W., “Behavior of welded girders with corrugated webs”, Ph.D. Thesis, University of Maine, Orono, USA, 1993.

[2] Leblouba, M., Junaid, M.T., Barakat, S., Altoubat, S. and Maalej, M., “Shear buckling and stress distribution in trapezoidal web corrugated steel beams”, Thin-Walled Structures, 113, 13-26, 2017.

[3] Eldib M.H., “Shear buckling strength and design of curved corrugated steel webs for bridges”, Journal of Constructional Steel Research, 65(12), 2129-2139, 2009.

[4] Timoshenko S.P. and Gere J.M., Theory of Elastic Stability 2nd ed., McGraw-Hill Book Company, New York, USA, 1961.

[5] Aggarwal K., Wu S.and Papangelis J., “Finite element analysis of local shear buckling in corrugated web beams”, Engineering Structures, 162, 37-50, 2018.

[6] Easley J.T. and McFarland D.E., “Buckling of light-gage corrugated metal shear diaphragms”, Journal of the Structural Division, 95(7), 1497-1516, 1969.

[7] Easley J.T., “Buckling formulas for corrugated metal shear diaphragms”, Journal of the Structural Division, 101(7), 1403-1417, 1975.

[8] Bergman S. and Reissner H., “Neuere probleme aus der flugzeugstatik–über die knickung von wellblechstreifen bei schubbeanspruchung”, Zeitschrift für Flugzeugtechnik und Motorluftschiffahrt, 20(18), 475-481, 1929.

[9] Hlavacek V., “Shear instability of orthotropic panels”, Acta Technica CSAV, 1, 134-158, 1968.

[10] Peterson J.P., Investigation of the Buckling Strength of Corrugated Webs in Shear, National Aeronautics and Space Administration, New York, 1960.

[11] Bergfelt A., Edlund B. and Leiva L., “Trapezoidally corrugated girder webs: shear buckling, patch loading”, Ing. et Arch. Suisses, 111, 22-27, 1985.

[12] Ziemian R.D., Guide to Stability Design Criteria for Metal Structures, 6th ed., John Wiley & Sons, New York, USA, 2010.

[13] El Metwally A. and Loov R.E., “Corrugated steel webs for prestressed concrete girders”, Materials and Structures, 36(2), 127-134, 2003.

[14] Machimdamrong C., Watanabe E. and Utsunomiya T., “Shear buckling of corrugated plates with edges elastically restrained against rotation”, International Journal of Structural Stability and Dynamics, 4(1), 89-104, 2004.

[15] Yi J., Gil H., Youm K. and Lee H., “Interactive shear buckling behavior of trapezoidally corrugated steel webs”, Engineering Structures, 30(6), 1659-1666, 2008.

[16] Bergfelt A. and Leiva-Aravena L., “Shear buckling of trapezoidally corrugated girder webs”, Division of Steel and Timber Structures, Chalmers University of Technology, Gothenburg, Publication S, 84(2), 1984.

[17] El Metwally A.S., “Prestressed composite girders with corrugated steel webs”, Ph.D.Thesis, University of Calgary, Calgary, 1998.

[18] Abbas H., Sause R. and Driver R., “Shear strength and stability of high performance steel corrugated web girders”, SSRC Conference, Seattle, USA, 361-387, 2002.

[19] Shiratani H., Ikeda H., Imai Y. and Kano K., “Flexural and shear behavior of composite bridge girder with corrugated steel webs around middle support”, Doboku Gakkai Ronbunshu, 2003(724), 49-67, 2003.

[20] Sayed-Ahmed E.Y., “Plate girders with corrugated steel webs”, Engineering Journal, 42(1), 1-13, 2005.

[21] Nie J.G., Zhu L., Tao M.X. and Tang L., “Shear strength of trapezoidal corrugated steel webs”, China Civil Engineering Journal, 67(2), 223-236, 2013.

[22] Elgaaly M., Hamilton R.W. and Seshadri A., “Shear strength of beams with corrugated webs”, Journal of Structural Engineering, 122(4), 390-398, 1996.

[23] Driver R.G., Abbas H.H. and Sause R., “Shear behavior of corrugated web bridge girders”, Journal of Structural Engineering, 132(2), 195-203, 2006.

[24] Moon J., Yi J., Choi B.H. and Lee H.E., “Shear strength and design of trapezoidally corrugated steel webs”, Journal of Constructional Steel Research, 65(5), 1198-1205, 2009.

[25] Hassanein M.F. and Kharoob O.F., “Shear buckling behavior of tapered bridge girders with steel corrugated webs”, Engineering Structures, 74, 157-169, 2014.

[26] Hassanein M.F., Elkawas A.A., EI Hadidy A.M. and Elchalakani M., “Shear analysis and design of high-strength steel corrugated web girders for bridge design”, Engineering Structures, 146, 18-33, 2017.

[27] Lekhnitskii S.G., Anisotropic Plates, Gordon and Breach Science Publishers, New York, USA, 1968.

[28] Batdorf S.B., A Simplified Method of Elastic-Stability Analysis for Thin Cylindrical Shells I: Donnell's Equation, Technical Report Archive Image Library, Langley Memorial Aeronautical Laboratory, Langley Field, USA, 1947.

[29] Xu Q. and Wan S., Design and Application of PC Composite Box Girder Bridges with Corrugated Steel Webs, China Communication Press, Beijing, China, 2009.

[30] Li S.M., Stability Theory, China Communications Press, Beijing, China,1989.

[31] Sause R. and Braxtan T.N., “Shear strength of trapezoidal corrugated steel webs”, Journal of Constructional Steel Research, 67(2), 223-236, 2011.

[32] ANSYS, ANSYS User’s Manual Revision 12.1, ANSYS Inc., Canonsburg, USA, 2012.

[33] Design Manual for PC Bridges with Corrugated Steel Webs., Research Committee for Hybrid Structures with Corrugated Steel Webs, 1998.

[34] Lindner J. and Aschinger R. “Biegetragfähigkeit von I-trägern mit trapezförmig profilierten stegen”, Stahlbau, 57(12), 1988.

[35] Peil, U., “Statische versuche an trapezstegtragern untersuchung der querkraftbeanspruchbarkeit, Institut fur Stahlbau”, Braunschweig (Germany): Technischen Universitat Braunschweig, 1998.

[36] Gil H., Lee S., Lee J. and Lee H., “Shear buckling strength of trapezoidally corrugated steel webs for bridges”, Transportation Research Record Journal of the Transportation Research Board, CD11-S, 473-480, 2005.

[37] Lindner J. and Huang B., “Beulwerte fur trapezformig profilierte bleche unter schubbeanspruchung”, Stahlbau, 64(12), 370-373, 1995.